Geological Society of America Special Papers

Field guide to exhumed paleochannels near Green River, Utah: Terrestrial analogs for sinuous ridges on Mars

Rebecca M.E. Williams, Rossman P. Irwin III, James R. Zimbelman, Thomas C. Chidsey, Jr. and David E. Eby

Geological Society of America Special Papers 2011;483;483-505
doi: 10.1130/2011.2483(29)

The Geological Society of America
Special Paper 483
2011

Field guide to exhumed paleochannels near Green River, Utah: Terrestrial analogs for sinuous ridges on Mars

Rebecca M.E. Williams[1], Rossman P. Irwin III[1], James R. Zimbelman[2], Thomas C. Chidsey Jr.[3], and David E. Eby[4]
[1]*Planetary Science Institute, 1700 East Fort Lowell Road, Suite 106, Tucson, Arizona 85179, USA*
[2]*Center for Earth and Planetary Studies, National Air and Space Museum, Smithsonian Institution, Independence Avenue at Sixth Street SW, MRC 315, Washington, DC 20013-7012, USA*
[3]*Utah Geological Survey, P.O. Box 146100, Salt Lake City, Utah 84114-6100, USA*
[4]*Eby Petrography and Consulting, 2830 West 9th Avenue, Denver, Colorado 80204, USA*

ABSTRACT

Multiple cemented channel-fill deposits from the Late Jurassic and Early Cretaceous, once buried beneath 2400 m of sediment, are now exposed at the surface in arid east-central Utah due to erosion of the less resistant surrounding material. This field guide focuses on examples near the town of Green River where there is public access to several different types of exhumed paleochannels within a small geographic region. We describe the geologic setting of these landforms based on previous work, discuss the relevance to analogous sinuous ridges that are interpreted to be inverted paleochannels on Mars, and present a detailed road log with descriptive stops in Emery County, Utah.

BACKGROUND

Geologic Setting for Exhumed Paleochannels in Emery County, Utah

Multiple exhumed paleochannels are located at the northern end of the Canyonlands section of the Colorado Plateau in east-central Utah (Young, 1960; Stokes, 1961; Derr, 1974; Rigby, 1976; Harris, 1980; Williams et al., 2007, 2009b). The exhumed paleochannels discussed here are within a 325 km^2 area and were originally deposited within an ~60 m.y. time span from the Late Jurassic to the Early Cretaceous (Figs. 1 and 2; note: descriptions for lithostratigraphic units within this region are in Appendix A). The sites vary in scale, morphology, depositional setting, and cement composition. However, the overall stages in the formation history of these features are similar (Fig. 3).

These exhumed paleochannels are examples of inverted topography, where a former topographic low (stream valley) transitions to a positive-relief feature as a consequence of differential erosion. Stream-laid deposits contain sediments that originated from a proto–mountain range to the west, the Sevier orogenic belt (Fig. DR1 available on CD-ROM accompanying this volume or in the GSA Data Repository[1]).

[1]GSA Data Repository Item 2011290, Figures DR1–DR14 and references, is available at www.geosociety.org/pubs/ft2011.htm, or on request from editing@geosociety.org, Documents Secretary, GSA, P.O. Box 9140, Boulder, CO 80301-9140, USA.

Williams, R.M.E., Irwin, R.P., III, Zimbelman, J.R., Chidsey, T.C., Jr., and Eby, D.E., 2011, Field guide to exhumed paleochannels near Green River, Utah: Terrestrial analogs for sinuous ridges on Mars, *in* Garry, W.B., and Bleacher, J.E., eds., Analogs for Planetary Exploration: Geological Society of America Special Paper 483, p. 483–505, doi:10.1130/2011.2483(29).

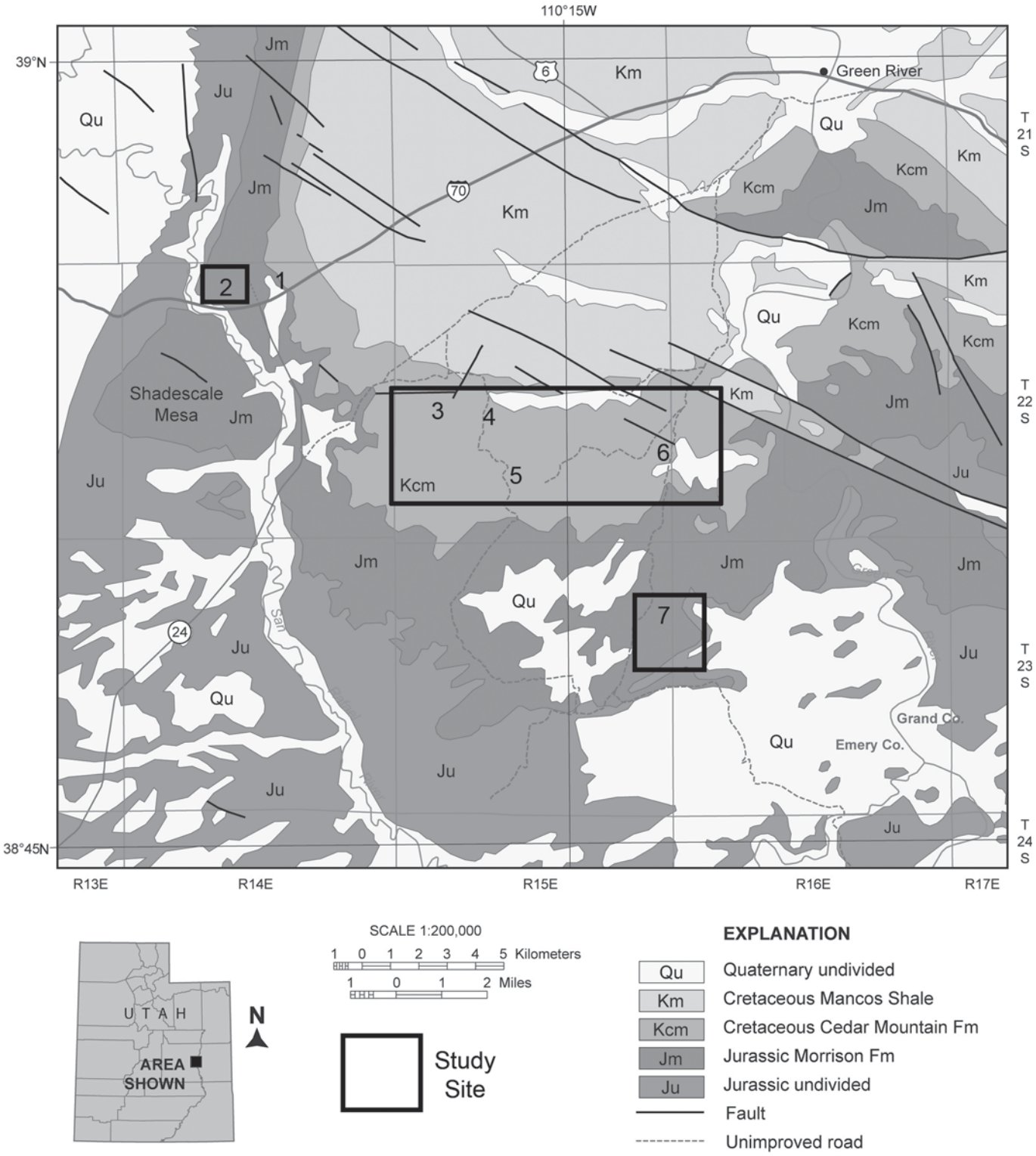

Figure 1. Inverted paleochannel sites described in the text are identified by rectangles on the geologic map of the study region in east-central Utah (figure from Williams et al., 2007; modified from Hintze et al., 2000). Numbers refer to stops in the road log.

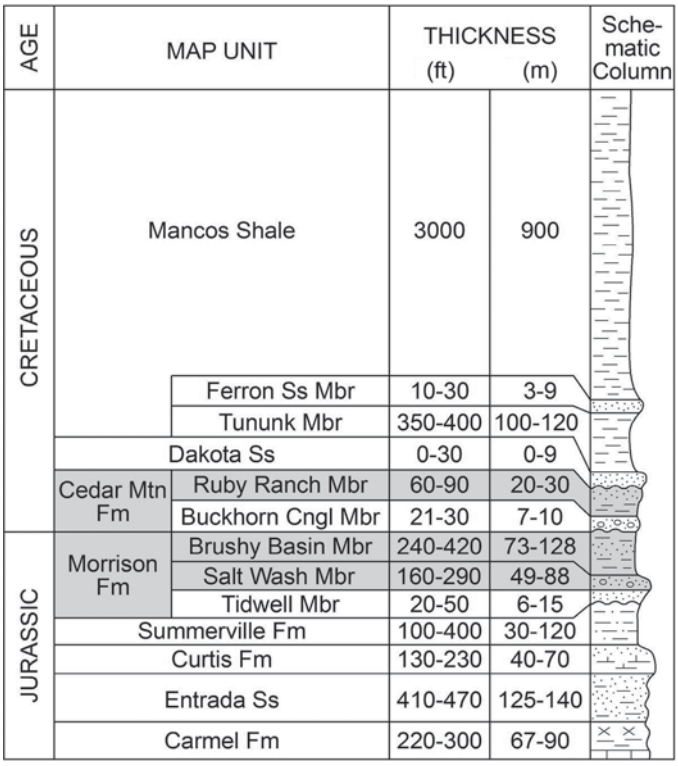

Figure 2. Stratigraphic column of lithologic units present within study region in east-central Utah (Williams et al., 2007). Thickness values for the lithologic units are based on the local region. Shaded units contain exhumed paleochannels. Ss—Sandstone. Figure is from Williams et al. (2007).

Carbonate and siliceous cements indurated the channel-fill deposits, making them more resistant to erosion than the surrounding material. During the Cretaceous, an interior seaway formed across west-central North America (Prothero et al., 2003, and references therein), and the marine Mancos Shale covered the channel deposits. Ultimately, the basin fill accumulated 2400 m of material within a variety of depositional environments (Nuccio and Condon, 1996; Nuccio and Roberts, 2003). The fluvial channel deposits remained buried for over 75 m.y. before the Laramide uplift and differential erosion of the surrounding units exposed the channel-fill deposits at the surface. Today, the paleochannels form ridges within three lithostratigraphic units: the Ruby Ranch Member of the Cedar Mountain Formation and both members of the Morrison Formation. The present-day arid climate over the Colorado Plateau has inhibited the development of thick soil horizons and pervasive vegetative cover, both of which would obscure these sedimentary bodies. The three-dimensional form of the exhumed paleochannels exposes sedimentary structures in multiple orientations. In this work, we refer to these ridges as paleochannels or simply channels.

Martian Fluvial Landforms

Over 200 candidate inverted channel sites, termed "sinuous ridges," have been identified on Mars based primarily on planimetric pattern (Williams, 2007). Comparative terrestrial studies are important for identifying the diagnostic criteria for distinguishing inverted channels from other ridge forms such as dikes and eskers (e.g., Howard, 1981), and for determining appropriate techniques for inferring the paleoenvironment associated with their formation. Illustrations of lessons learned from terrestrial analogs, including the inverted paleochannels near Green River, Utah, are presented in the road log.

Deciphering the history of water on Mars is complicated by the fact that liquid water is unstable there under current atmospheric conditions. At most locations on Mars, year-round surface temperatures and pressures are below the triple point of water (273 K, 0.61 kPa), so liquid water spontaneously boils and/or freezes (Haberle et al., 2001). However, for nearly four decades, scientists have recognized landforms that record past surface flow of water on Mars (Mars Channel Working Group, 1983; Carr, 1996). Principal among these landforms are valley networks, which are analogous to terrestrial rivers and are concentrated on the ancient southern highlands (e.g., Carr and Clow, 1981; Hynek et al., 2010). In addition, alluvial deposits at the mouths of some valleys may mark former lacustrine sites (e.g., Malin and Edgett, 2003; Moore and Howard, 2005; Cabrol and Grin, 2010; Fig. 4). Evidence from the geomorphology of valley networks (Baker and Partridge, 1986; Williams and Phillips, 2001; Harrison and Grimm, 2005, Howard et al., 2005), decline in weathering rates (Golombek et al., 2006), and global mineralogy (Bibring et al., 2006) supports a transition from clement climate conditions in which water was abundant on the surface early in the Noachian Period (4.55 to ca. 3.7 Ga) to more arid conditions late in the Noachian and into the Hesperian Period (ca. 3.7 to ca. 3.0 Ga). Even after the climate became more arid, the Martian surface continued to be modified by very short duration fluvial activity, including large-scale outflow channels formed by catastrophic floods (e.g., Baker, 1982) and small gullies that may be active today on some steep midlatitude slopes (e.g., Malin and Edgett, 2000; Malin et al., 2006; Harrison et al., 2009; Dundas et al., 2010). Debate persists regarding the duration of Martian climates that were warmer and wetter than present and the nature of the transition, i.e., whether there were long-term secular changes or brief climate excursions, particularly in the absence of abundant deep weathering products. Temporary climatic optima lasting a few decades could be obtained from volcanic outgassing of SO_2 (Halevy et al., 2007; Johnson et al., 2008) or interim greenhouse associated with large impact events (Carr, 1989; Segura et al., 2002, 2008).

Sinuous ridges, some of which are interpreted to be fluvial landforms preserved in inverted relief (Figs. 4–6; e.g., Tanaka and Kolb, 2001; Williams et al., 2005; Pain et al., 2007), provide another indication of flowing water on the Martian surface. Preliminary work has shown that these landforms are present on terrain that spans from the Noachian to the more recent Amazonian Periods (<3.0 Ga) and are, therefore, an important record of the environmental conditions over the entire geologic history of Mars (Williams, 2007). For example, inverted fluvial channels

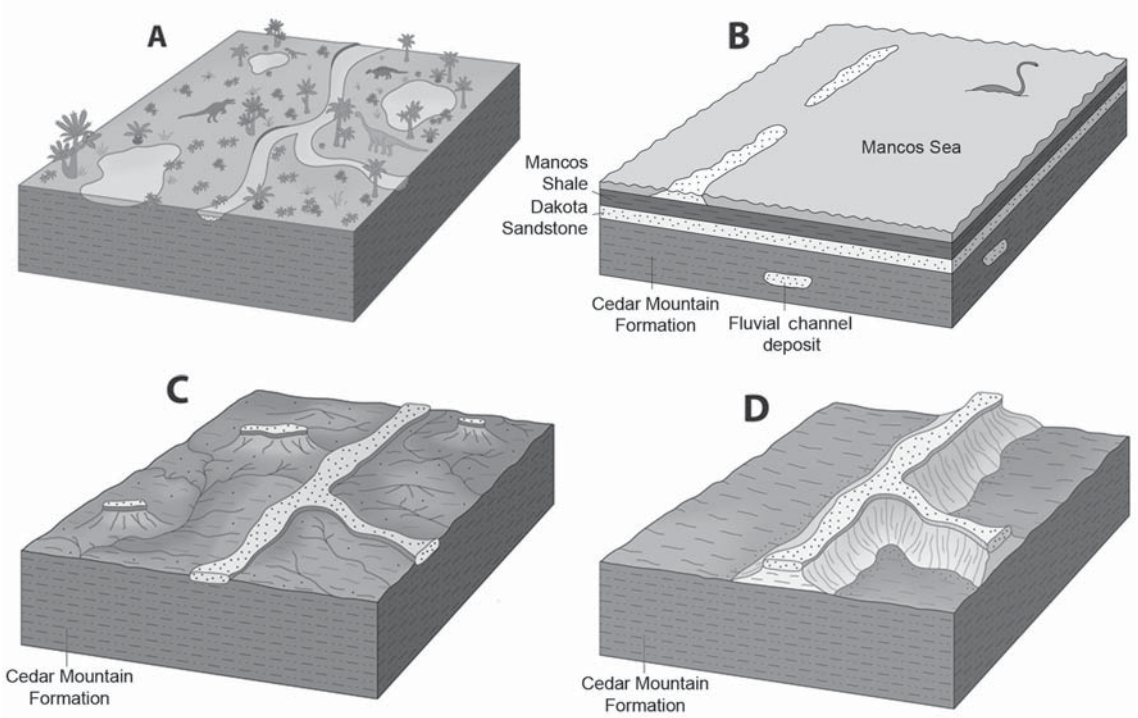

Figure 3. Block diagrams illustrating the phases of formation in developing inverted paleochannels (figure from Williams et al., 2007). Although his example is for inverted paleochannels within the Ruby Ranch Member of the Cedar Mountain Formation, located in the central rectangle in Figure 1, the overall stages are generally applicable to other inverted paleochannels sites discussed in this field guide. (A) Depositional settings—alluvial plain, fluvial channel, and floodplain—in the study region during the Early Cretaceous. The schematic includes Aptian- to middle Albian–age dinosaurs and plants. (B) In the Late Cretaceous, the study region was beneath a shallow sea. Ultimately, the region was buried by ~2400 m of sediments and remained buried for over 75 m.y. (C) Subsequent uplift and erosion from the middle Tertiary to the present stripped away the overburden, revealing the paleochannel deposits at the surface today. (D) Present-day expression of inverted paleochannels is preserved as a topographic ridge ~35 m above the surrounding plains.

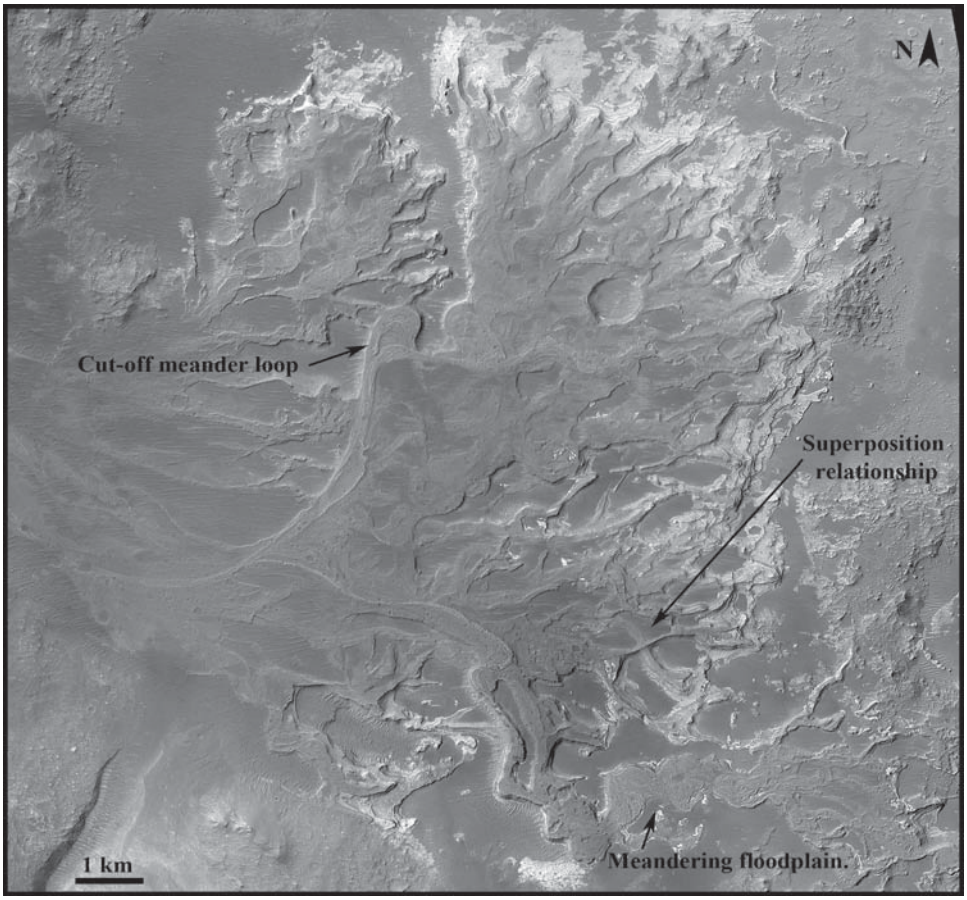

Figure 4. A Mars Orbital Camera (MOC) image mosaic of portion of Eberswalde crater (24.3°S, 33.5°W). At this site, a multilobe distributary fan complex composed of crosscutting ridges is interpreted to be a deltaic deposit preserved in inverted relief, likely due to wind erosion (Malin and Edgett, 2003; Moore et al., 2003). Individual scroll bars within the cutoff meander loop are evidence of channel migration. Superposition relationships are preserved where late-stage channels formed on top of older channels. Image credit: National Aeronautics and Space Administration (NASA)/Jet Propulsion Laboratory (JPL)/Malin Space Science Systems.

on the northern Valles Marineris plateau have been cited as evidence for episodic fluvial activity after the end of the Noachian Period, well after the cessation of widespread formation of valley networks on the cratered highlands (Fig. 5; Mangold et al., 2008). Similar landforms in the Aeolis–Zephyria Plana region (Fig. 6) record paleoflows that occurred sometime between the Late Hesperian and middle Amazonian (Burr et al., 2009). However, it is unknown whether these record short-term climate changes or regional variations in aqueous processes. Determining the relative timing and duration of fluvial activity on Mars is critical to understanding climate variations and assessing the potential for life to have developed.

ROAD LOG

This road log highlights paleochannels in the Morrison and Cedar Mountain Formations along a loop from the city of Green River, Utah (Fig. 7). The stops provide a variety of vantage points to examine these landforms. Each stop includes a description of the features at that location as well as discussion of direct relations or insight to inferred Martian inverted channels.

All sites discussed within this field guide are on public lands managed by the U.S. Bureau of Land Management (BLM). Latitude and longitude coordinates are referenced to the World Geodetic System 1984 datum (National Imagery and Mapping Agency Technical Report, 2000). A four-wheel-drive vehicle is recommended to complete the loop route because road quality varies from paved roads, to graded dirt roads, to unmaintained dirt roads. An abridged, alternate route suitable for all vehicles that includes stops at inverted paleochannels from each formation is presented in Appendix B.

Mile 0.0. Begin at U.S. Post Office located at the corner of Clark and Main Streets in Green River. Zero odometer. Head west on Main Street and enter Interstate 70 (I-70) westbound.

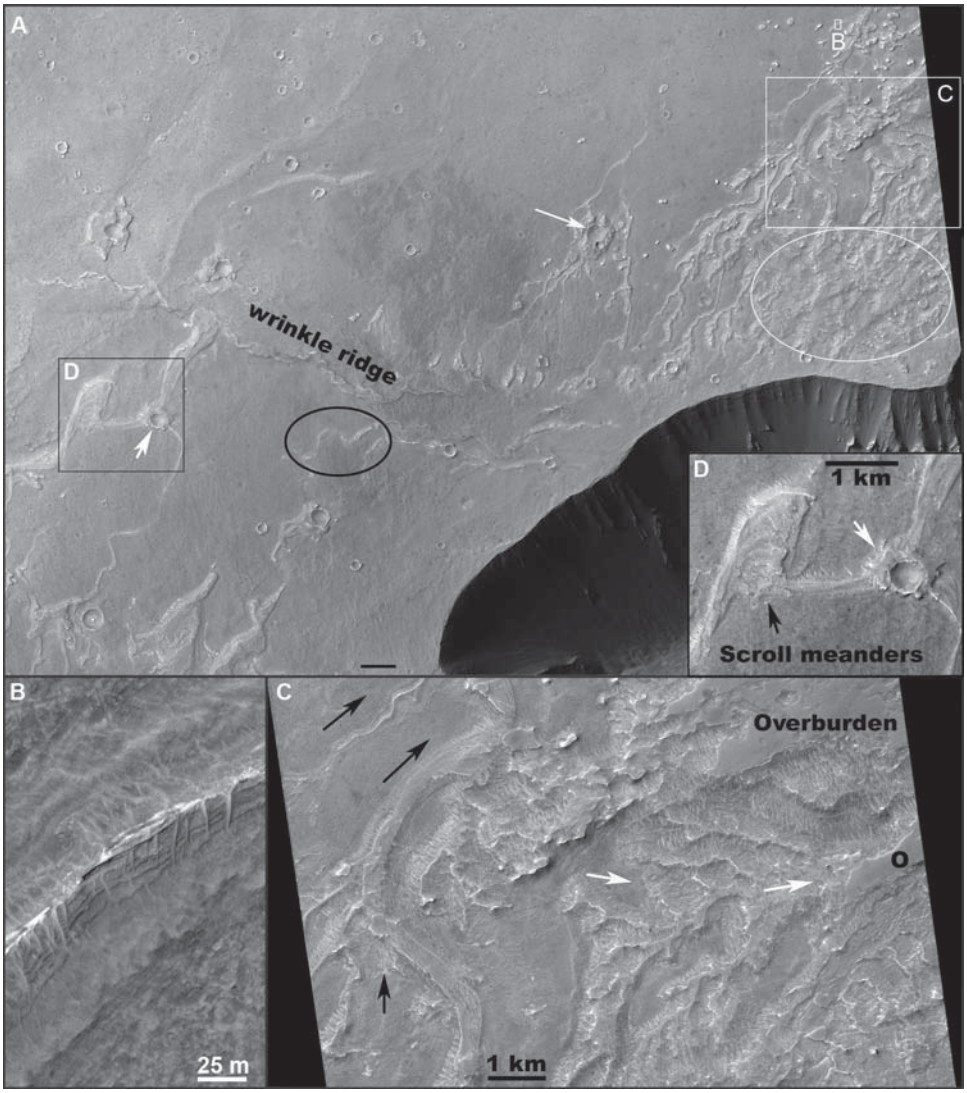

Figure 5. Branching ridge networks preserved on Lunae Planum near Juventae Chasma have among the highest drainage density for fluvial landforms observed on Mars. Many of the branching ridge networks have a dendritic pattern (particularly in upper right of panel A). However, there are isolated cases of meandering channel paths, such as the preservation of apparent meander migration in panel D. (A) The influence of topography on channel course is evident at the black oval, which highlights a meandering ridge; when the channel was active, the vand the flow direction changed to the southeast, parallel to the ridge. These ridge networks have been exhumed. Craters obscure a portion of ridge network (white arrows in A and D), and are remnants of strata that were once more regionally extensive but are now only locally preserved. (B) Layering is evident beneath the cap rock along sections of the sinuous ridge. (C) Two ridge networks with different planimetric pattern, flow orientation, and position within the stratigraphic rock record. At left, there is a broadly branching network with a broadly sinuous trunk channel that flowed to the north (black arrows). To the south, this ridge unit is buried by a rugged material (white circle in panel A). At right, there is a dendritic branching network with an inferred flow direction to the east (white arrows); the distal portion of this network is buried beneath a flat-topped, pitted mantle unit labeled "Overburden" and "O." Panels A and C are subframes of ConTexT (CTX) Camera image P01_001337_1757 in southeastern Lunae Planum near 4°S, 63°W, while panels B and D are subframes of High Resolution Imaging Science Experiment (HiRISE) image PSP_006981_1760; illumination is from lower left for all panels.

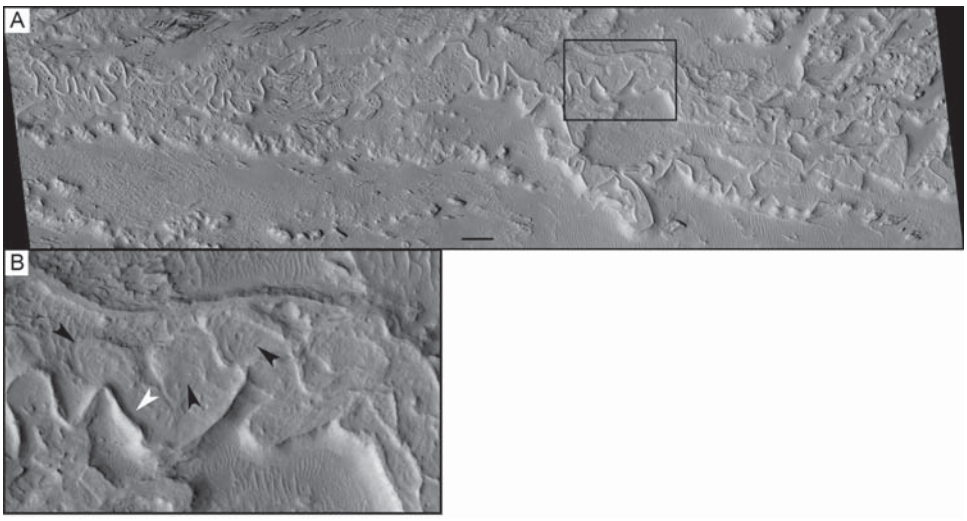

Figure 6. (A) A multilevel sinuous ridge in the Aeolis–Zephyria Plana region. The top ridge has a curvilinear and meandering path. This ridge is superposed on top of a broad mesa, which is interpreted as a former floodplain from an earlier flow. Black box is the approximate location of panel B. (B) Subparallel, curved lineations (black arrows) are present on the surface of the mesa. These are interpreted as scroll meanders that formed in a laterally migrating meandering stream. White arrow marks sinuous ridge that superposes the flat mesa and is inferred to mark a later fluvial event. See Burr et al. (2009) for further discussion. Subframe of ConTeXt Camera (CTX) image P06_003215_1752 near 5°S, 205°W. Illumination is from lower left.

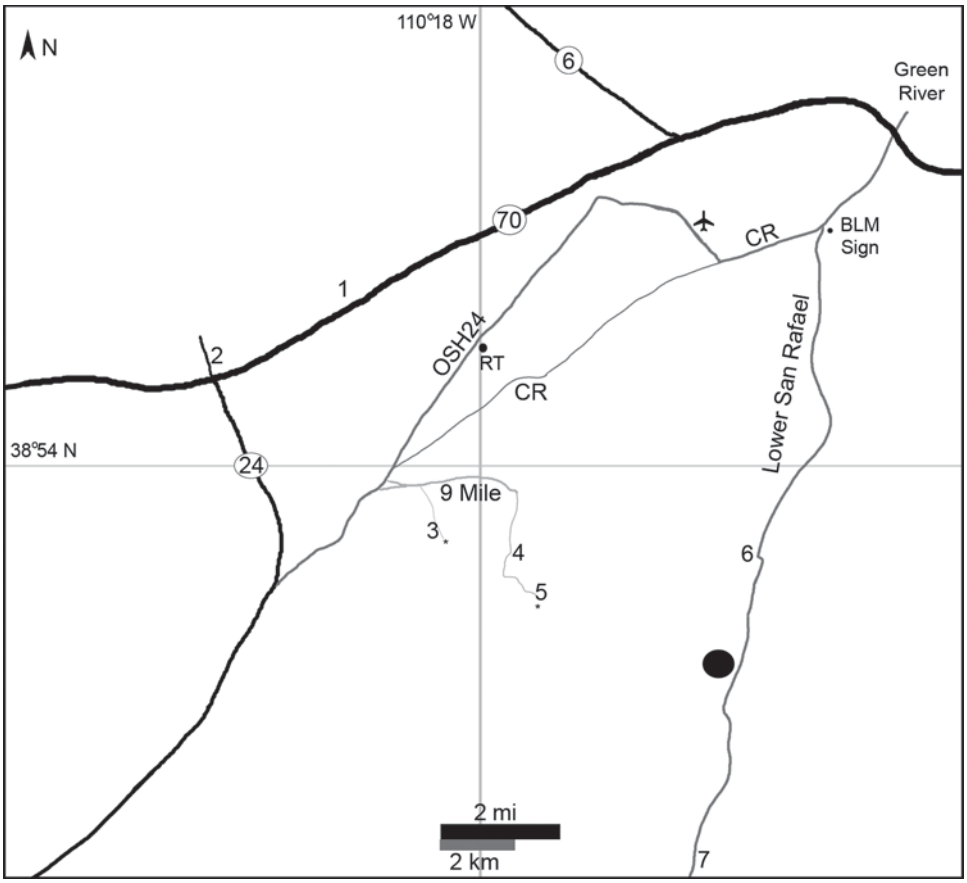

Figure 7. Sketch map of roads referred to in the road log. Thickness and color of roads are an indication of relative quality. Note that we found the paved road OSH24 preferable to County Road, a dirt road, and it resulted in a much faster transit time to reach the eastern field sites. Abbreviations: OSH24—Old State Highway 24, CR—County Road, RT—Radio Tower, 9 Mile—Nine Mile Reservoir Road; BLM—Bureau of Land Management. Asterisks mark the farthest extent we explored on unmaintained dirt roads.

Mile 6.6 (6.6 incremental miles). San Rafael Swell is visible on the horizon.

Background: Brushy Basin Member Paleochannels

Derr (1974) mapped three isolated paleochannel segments interpreted to be a floodplain channel complex within the Brushy Basin Member of the Morrison Formation west of Green River along Interstate 70 (Fig. 8; Fig. DR2 [see footnote 1]). He documented three short, low-sinuosity channel segments (numbered in order of their stratigraphic position) that are light-gray in color but weather red-brown. Flow direction is varied, reflecting the low-relief depositional setting; the channels at stop 1 (channels 2 and 3) typically flowed to the

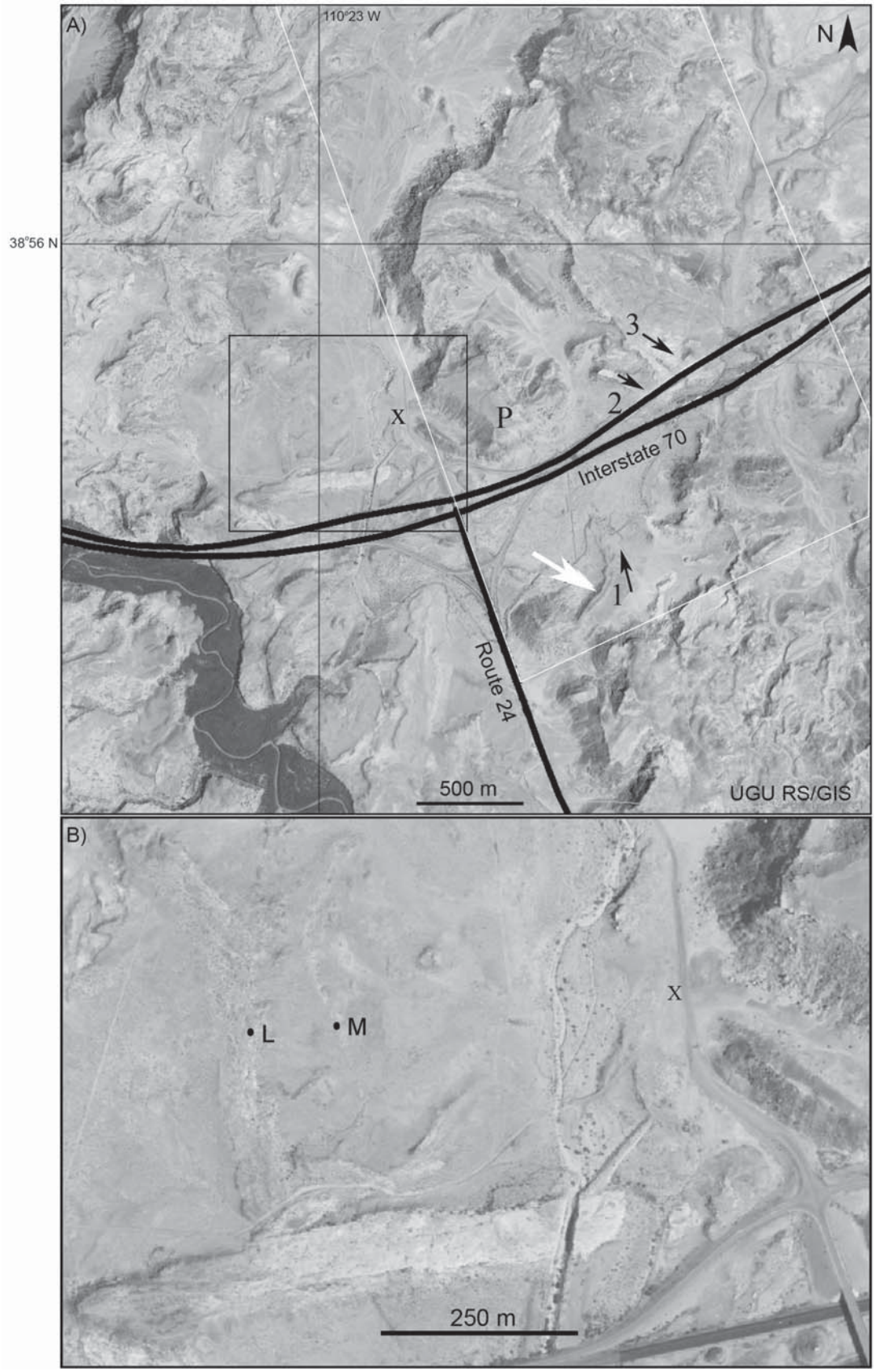

Figure 8. (A) Aerial photomosaic (1 m/pixel, acquired in 2006) of inverted paleochannel sediments in the Late Jurassic Brushy Basin Member of Morrison Formation. White box is approximate outline of Derr's (1974) study site, and his nomenclature for channel systems is denoted by numbers. White arrow points to channel 1; channels 2 and 3 are marked by numbers. Black arrows indicate paleoflow direction determined by Derr (1974). "P" is the location from which Figures DR2 and DR4 were acquired (see text footnote 1). "x" denotes the parking location. Black box is area enlarged in bottom panel. Note that 500 m is approximately equivalent to 0.3 mile. (B) Subsection of top image enlarged to highlight the region near stop 2. Thin sections were made from samples collected at two inverted channel locations marked by lettered dots (L and M) and are illustrated in Figure DR5 (see text footnote 1). Annotated image is from Virtual Utah (http://earth.gis.usu.edu/utah), Remote Sensing and GIS Laboratory, Utah State University, Logan.

southeast. The channel segments here reflect an original channel profile that was broad and shallow, with width-to-depth ratios of 10:1 for channel 1 and up to 20:1 for channels 2 and 3 (Derr, 1974). Derr (1974) estimated former stream gradients of 0.4 m/km and used channel dimensions to estimate average annual discharge rates of 10–120 m^3/s.

Mile 12.0 (5.4 incremental miles). Stop 1. Road cut through Brushy Basin Member paleochannels (Derr, 1974) (38°55′44″N, 110°21′50″W, near 150 mile marker; Fig. 8; Fig. DR2 [see footnote 1]). Care should be used in pulling off the freeway to examine the road cut on the north side of I-70, where there is a nearly perpendicular exposure of channel segments within the Brushy Basin Member. Additional exposures of paleochannels are present ~0.2 km west of the stop coordinates. This stop is a good introduction to inverted paleochannels and affords a number of viewing geometries for these landforms. By climbing atop the outcrop, one can view the channel-fill material in plan view, extending to the northwest as a lighter-toned path.

Channel segments are generally lens-shaped in cross section with convex bases. Channels range in thickness from a few centimeters to 10 m and can extend to nearly 100 m in width. Channels exhibit an overall upward-fining sequence from conglomeratic bases to medium and fine sand at their upper exposed surfaces. The size of sediment and cross-beds decreases upward through the sequence. Horizontal bedding predominates in the shale and siltstone, but micro–cross-lamination, reflecting deposition in low-energy currents on the interchannel floodplain, also occurs within these beds.

Derr (1974) identified three major types of bedding within the channel segments: planar (tabular) cross-beds, trough-shaped cross-beds (the predominant bedding type on exposed surfaces), and horizontal stratification (current lamination, which is only exposed in cross section). Channels typically exhibit an upward-fining vertical sequence (from base to upper surface) that is consistent with a point-bar sequence (Visher, 1965; Harms and Fahnestock, 1965): cross-bedded pebble conglomerate, cross-bedded sandstone, horizontally stratified sandstone, and cross-bedded sandstone. Cross-beds are separated by sand, reflecting continuity in flow conditions as the channel migrated laterally. These inverted paleochannels preserve a meander (point-bar) complex.

Discussion: Overview of Inverted Paleochannels

This stop illustrates exposures of inverted channels in three dimensions and provides an overview of the types of features and attributes that are helpful in discerning these landforms from ridges that form from other mechanisms, such as subglacial stream deposits (eskers) or volcanic dikes. The interpretation of some Martian sinuous ridges as inverted channels relies on several lines of evidence. The planimetric pattern for Martian ridges can be quite compelling in inferring a fluvial origin, particularly for examples of branching ridge networks with high Strahler order (Fig. 5) or meandering courses (Fig. 6). Contextual relationships are also useful in assessing potential formation models for Martian sinuous ridges. Some ridges are continuous with valley networks, bolstering the interpretation of a fluvial system (Fig. DR3). Additional observational criteria for identifying inverted channels in remotely sensed data include planimetric pattern, surface textures, and composition. We continue to explore aspects of the morphology that are diagnostic of inverted paleochannels in the following stops.

Proceed east on I-70 to the next exit for Route 24. Turn right at the end of the exit ramp. The road is paved for only a short distance, and at the transition to a graded dirt road, there is ample room to park. It is a short walk (<500 m) west to stop 2.

Mile 13.0 (1.0 incremental miles). Stop 2. Additional inverted paleochannel examples from the Brushy Basin Member (38°55′38″N, 110°22′44″W). Two single-thread exhumed channels within the Brushy Basin Member are located just outside of Derr's (1974) study region (Fig. 8B). The surface of these subtle relief features (<2 m) is sparsely vegetated and exhibits trough cross-beds that indicate paleoflow direction to the south (Fig. 9; Fig. DR4). The quartz grains in these channel segments are bound by silica overgrowths and calcite cements (Fig. DR5; Williams et al., 2009a), consistent with the results reported by Derr (1974) for exhumed paleochannels of comparable age located ~1 km to the east (e.g., stop 1).

Discussion: Cementation as an Indurating Agent

Landscape inversion occurs when features possess or develop greater resistance than the surrounding terrain and are preferentially preserved via differential erosion. Multiple scenarios can lead to this increased resistance, including geochemical cementation, clast armoring, or infilling by a resistant material (such as lava). The inverted paleochannels in this field guide are examples of cemented channel-fill materials preserved as ridges following denudation of the landscape.

Cementation has been argued as the likely cause of induration in most Martian sinuous ridges based on (1) the observation of surface cementation at rover sites, which suggests that it is a ubiquitous process on Mars as it is on Earth, (2) the similarities in surface morphology with terrestrial analogs (Williams et al., 2007, 2009b; Pain et al., 2007; Burr et al., 2009, 2010), and (3) the lack of recognizable volcanic sources proximal to many of the sinuous ridges. Depending on the cementation mechanism (discussed further at stop 7), the resulting indurated material may be confined to alluvium, or it may also involve materials adjacent to the channel. Cementation has the potential to preserve sedimentary structures (e.g., scrollbars, cross-bedding, etc.), in contrast to lava flows, which may display flow lineations, pressure ridges, or columnar jointing. Very few sinuous ridges have been proposed as lava-capped (e.g., an example near Mangala Valles; Rhodes, 1980). Alternative formation mechanisms for Martian inverted channels are discussed in detail by Pain et al. (2007) and Burr et al. (2010).

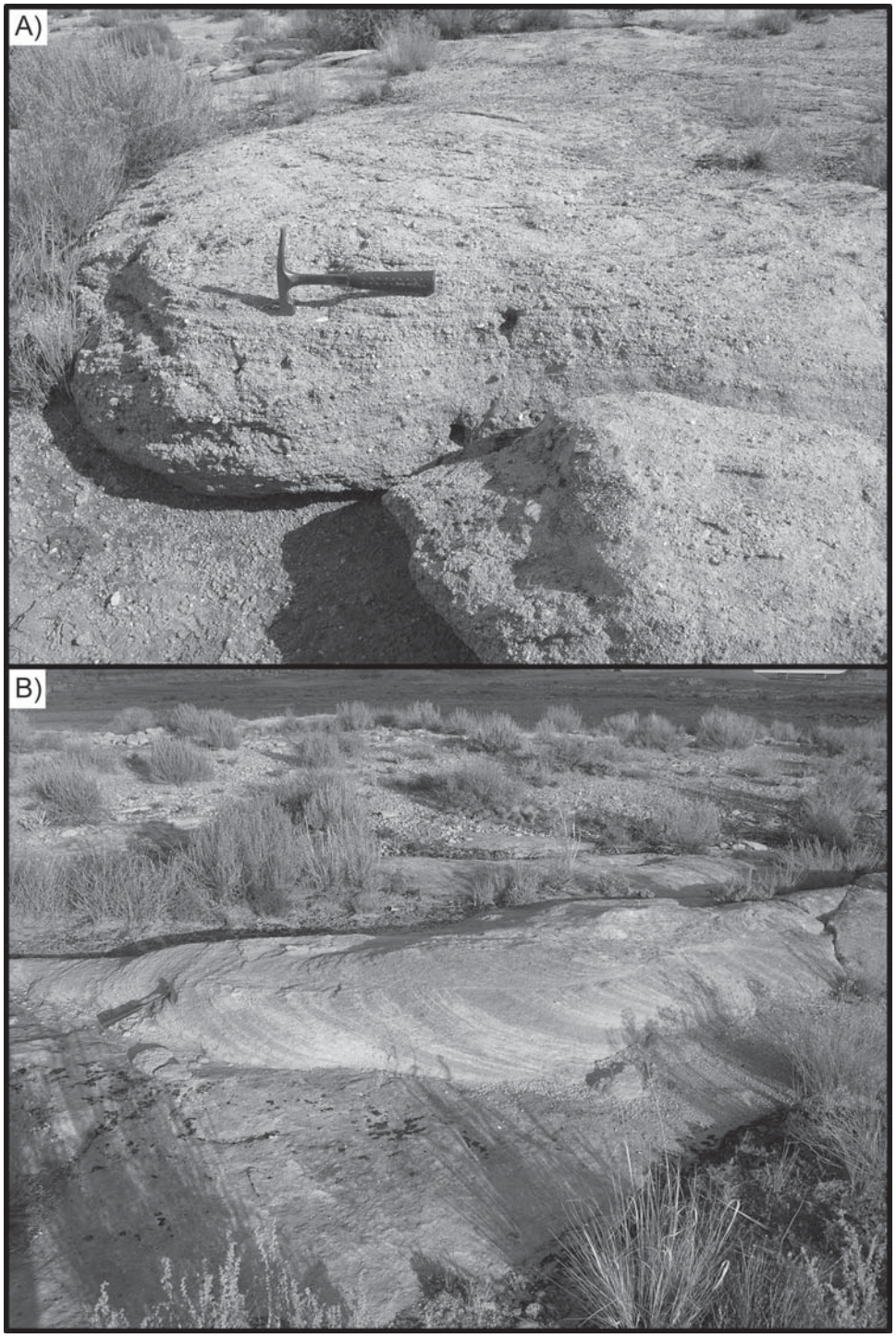

Figure 9. (A) Coarse-grained cemented stream deposits in the Brushy Basin Member. Hammer for scale. Photo by R. Williams. (B) Large-scale trough cross-beds on the surface indicate a paleoflow direction to the south. Hammer for scale. Photo by R. Williams.

Direct detection of the cement composition in a Martian sinuous ridge has not yet occurred due in part to pervasive dust cover and instrument resolution. However, elemental and mineral signatures from rover and orbital instruments have identified several potential cements including sulfates (jarosite, gypsum, epsomite), iron oxides (hematite), silica, clay (nontronite), halides, chlorides, sulfate polyhydrates, and carbonate (e.g., Bandfield et al., 2003; Landis et al., 2004;

Bibring et al., 2005, 2006; Glotch et al., 2006; Ehlmann et al., 2008; Osterloo et al., 2008; Morris et al., 2010).

Proceed on Route 24 south. Immediately after crossing I-70, look to the left to see another inverted paleochannels from the Brushy Basin Member. In contrast to the paleochannels at stop 1, Derr (1974) interpreted this isolated channel segment (channel 1, Fig. 8A) to have formed primarily via avulsion in a floodplain or deltaic setting. Although this site is not easy to explore due to fences, it is interesting to note the observations of Derr (1974) that led him to conclude that this stream was overloaded with sediment, did not meander, and accumulated sediment in pulses rather than continuously. Overall, the sediments are poorly sorted. In cross section, channel 1 has an irregular vertical sequence consisting of cross-stratification and horizontal stratification cosets that vary widely in scale. Cross-bed sets are often separated by clay and silt, reflecting intermittent flow conditions.

Mile 16.9 (3.9 incremental miles). Turn left on Old State Route 24 (also called County Road 1007), a paved road.

Mile 19.4 (2.5 incremental miles). Turn right onto Nine Mile Reservoir Road (also called County Road 1043), a dirt road. A four-wheel-drive (4WD) vehicle is recommended for this stop. Alternatively, proceed on Old State Route 24 to stop 6, as detailed on the CD-ROM accompanying this volume and in the Data Repository (see footnote 1). If you have a global positioning system (GPS) unit, it is helpful to mark the position of each of the turns en route to stop 5, because you will retrace this path.

Mile 20.1 (0.7 incremental miles). Turn right on an unnamed dirt road (possibly Nine Mile Loop Road). After 0.3 mile (500 m), bear right at junction.

Background: Ruby Ranch Member Paleochannels

The longest known inverted paleochannel system on the Colorado Plateau consists of four multi-kilometer-length conglomerate/sandstone-capped ridges, and numerous shorter ridge segments within the Ruby Ranch Member of the Cedar Mountain Formation (Fig. 10). Young (1960) and Stokes (1961) briefly mentioned these channel deposits prior to the sedimentological study conducted by Harris (1980), who identified four main segments that he labeled A through D. The total complex spans 12 km, and individual paleochannel segment lengths range from 4.5 to 8 km, but continuity can be inferred between some adjacent segments. Channel form is generally linear, although some sections exhibit low sinuosity ratios between 1.2 and 1.5. Based on the paleochannel pattern, Harris (1980) interpreted meandering streams to have formed these segments. Sedimentary structures are exposed in plan view and cross section (Fig. 11). Cross-bed sets in the sandstone are up to 2 m in height and are expressed on the mesa surfaces as scalloped, broadly concave-downstream features. Sedimentary structures are absent in the basal conglomerate beds (Fig. DR6). Paleoflow direction was to the north and east, parallel to the local axial trend of the channel deposits where cross-bedding orientation was measured (Harris, 1980). Harris (1980) estimated annual discharge rates ranging from 20 to 620 m^3/s based on channel dimensions.

Although originally characterized as carbonate-cemented inverted channels in prior publications (e.g., Harris, 1980; Lorenz et al., 2006), silica cement was reported by Lorenz et al. (2006). Newsom et al. (2010) identified silica as a significant component of the cement by microprobe examination of cemented sediments. Petrographic examination of these cemented channel-fill materials has revealed that silica is the dominant binding agent, with minor, late-stage calcite cement (Fig. DR7 [see footnote 1]; Williams et al., 2009a). There are three generations of silica cement that formed under near-surface conditions, likely via evaporation.

These are the youngest exhumed paleochannel deposits discussed in this paper and exhibit the highest relief, up to 40 m above the surrounding plains, with cemented channel sediments evident in the top 2–10 m of the ridges. Using the present relief of these features and long-term average erosion rates for the region (Nuccio and Condon, 1996; Nuccio and Roberts, 2003), Williams et al. (2007) estimated that their maximum surface re-exposure age is 650,000 yr.

Mile 21.0 (0.9 incremental miles). Stop 3. Sinuous course of inverted paleochannel A (Harris, 1980) in the Ruby Ranch Member (38°53′12″N, 110°18′26″W). This section of channel A is noteworthy for its highly sinuous course (Fig. DR8), in contrast to the more linear channel sections that are preserved in this area. The road passes through a water gap in the inverted channel. Walk east along the ridge for ~0.5 km, where there is a northern spur. Superposition relationships indicate that this is a remnant of a former channel position, not a tributary to channel A. Interestingly, extension of this older channel has been lost on the south side of the escarpment due to erosion (Harris, 1980). A modern, well-developed drainage network has developed on the northern side of the ridge.

Discussion: Landscape Evolution

Rocks now exposed in the Colorado Plateau were below sea level during the Late Cretaceous and are presently at an average elevation of 2.2 km. There is disagreement over the mechanisms and rate of uplift for the Colorado Plateau during the 80 m.y. interval since the last marine deposition; however, there appears to be consensus that the uplift rate was rapid over the last several million years (Ruddiman et al., 1989; Sahagian et al., 2002). The major drainage systems of the Colorado Plateau responded to the dramatic base-level change. Large volumes of material were transported through the ancestral drainage network of the Colorado River (e.g., Hunt, 1969; Lucchitta, 1990), ultimately resulting in the exhumation of the paleochannel deposits in the Morrison and Cedar Mountain Formations (Fig. 3).

The modern drainage development at this site is a visual reminder of the differences in the erosive histories on Earth and

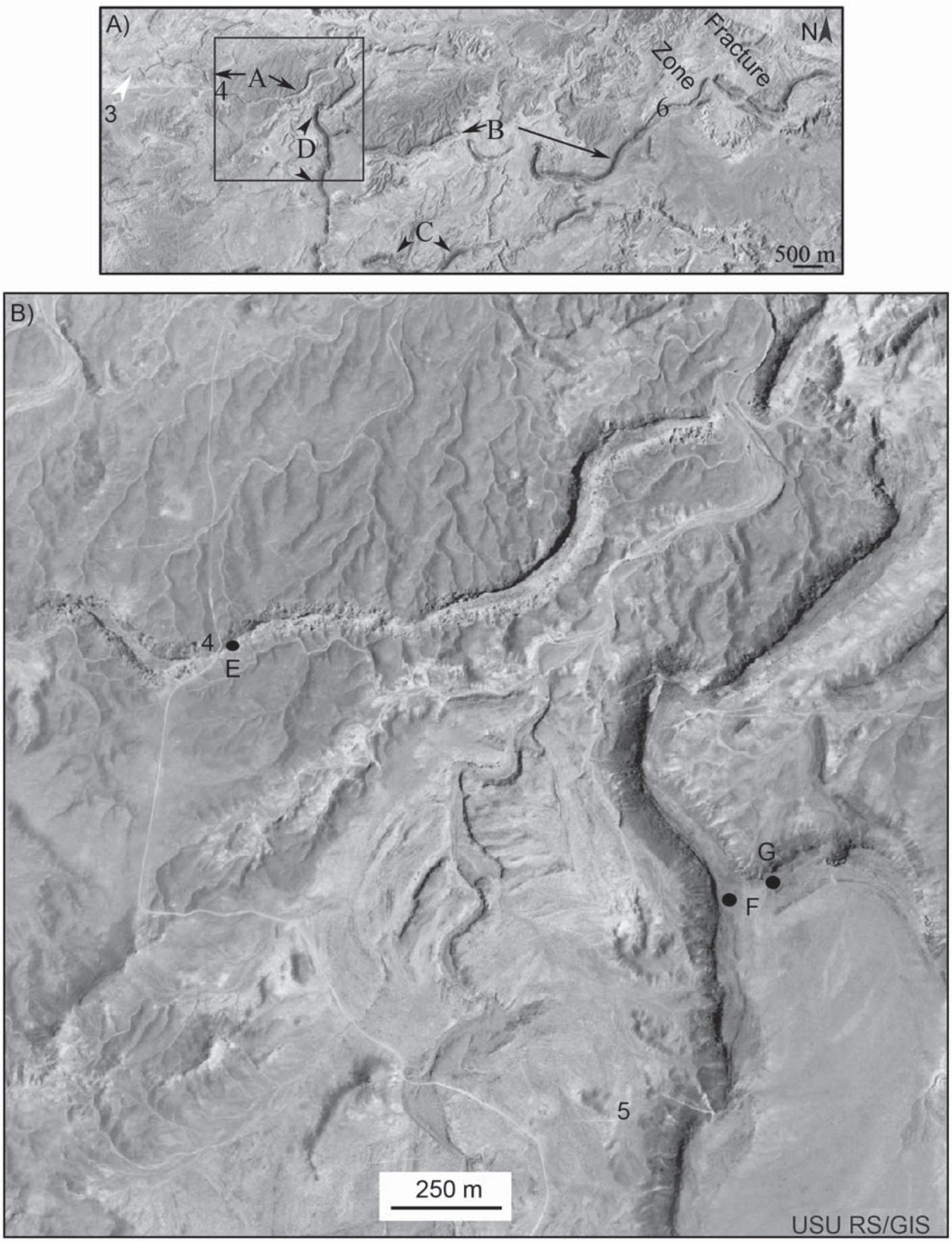

Figure 10. (A) Aerial photomosaic (1 m/pixel, acquired in 2006) of inverted paleochannel sediments that are part of the Early Cretaceous Ruby Ranch Member of the Cedar Mountain Formation. See central rectangle in Figure 1 for site location. Channel segments are labeled according to Harris (1980). Field stops 3–6 are marked by numbers. Fracture zone is most evident to the east. White arrow (above number 3) marks water gap. Note that 500 m is approximately equal to 0.3 mile. (B) Enlargement of section of image to highlight the region in the road log. Thin sections were made from samples collected from locations marked by lettered dots (E–G) and are illustrated in Figure DR6 (see text footnote 1). At field stop 5, the destination of the walk is near letter F.

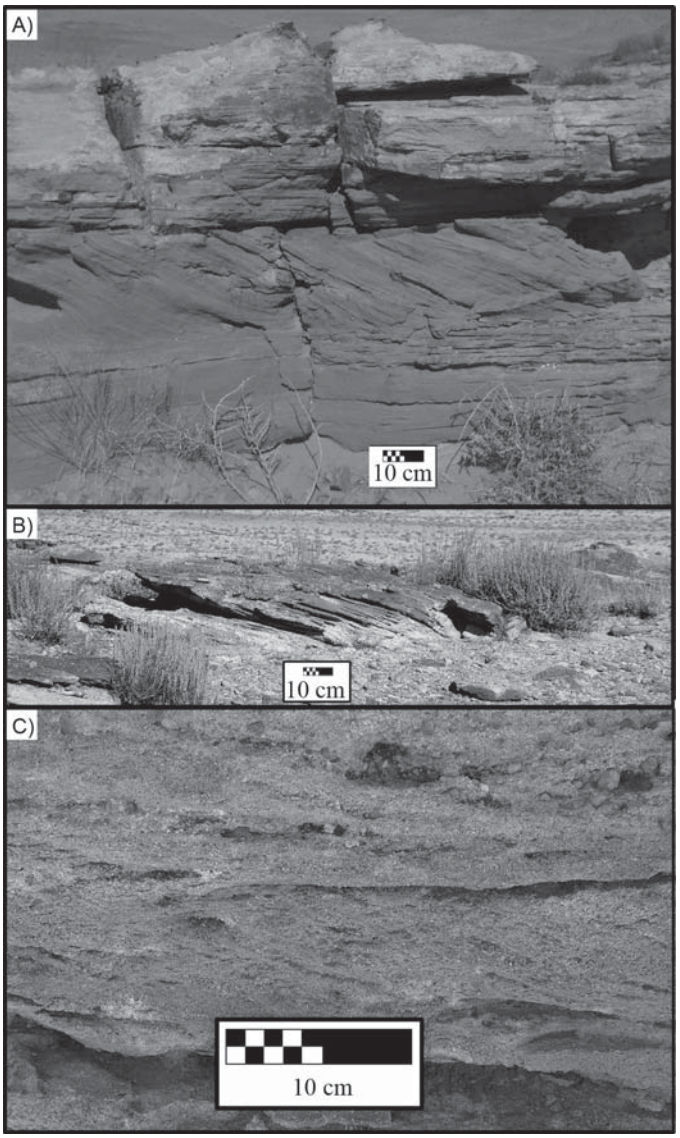

Figure 11. (A) Outcrop in channel D with cross-strata interbedded with horizontal stratification. Photo by J. Zimbelman. (B) Large-scale cross-bedding in channel D that is evidence of lateral accretion, likely of a point-bar deposit. Photo by R. Williams. (C) Climbing ripples in a vertical exposure of a point-bar deposit. Ripple marks are rarely found on paleochannel surfaces. Photo by R. Williams.

Mars. In contrast to the Utah inverted paleochannels, which were exhumed by fluvial erosion, wind was likely the dominant erosive agent responsible for creating sinuous ridges on Mars. Rates of eolian erosion vary greatly depending on many factors, including wind velocity, atmospheric density, surface roughness, rock strength, sediment size, and availability of mobile material to abrade. Estimates of long-term erosion rates from surface landers and rover observations on Mars indicate minimal deflation of plains basalt, 10^1–10^2 nm per thousand years (k.y.) for at least the past ~2 b.y., which is consistent with a dry and desiccating environment (Golombek and Bridges, 2000; Golombek et al., 2006). These erosion rates are 2–5 orders of magnitude lower than minimum continental denudation rates on Earth and indicate that liquid water was not an active erosional agent (Golombek et al., 2006). Significantly higher denudation rates (10^5–10^7 nm/k.y.) based on crater degradation studies were determined for the first billion years of the planet's history (e.g., Craddock and Maxwell, 1993; Craddock et al., 1997; Hynek and Phillips, 2001). Recent simulations of Martian wind erosion based on general circulation models (GCMs) suggest that higher long-term eolian erosion rates (10^6–10^7 nm/k.y.) are possible regionally in the past 1 b.y.; these rates are consistent with removing several kilometers of easily eroded fine regolith within 100 m.y. (Armstrong and Leovy, 2005). Wind erosion (mechanical weathering) is less efficient at weathering indurated materials than fluvial erosion (chemical and mechanical weathering). Therefore, the dry environment on Mars may be more conducive to preserving sinuous ridges at the surface for longer periods of time (millions if not billions of years) than on Earth (examples in this field guide have been exposed at the surface for a maximum of a few hundred thousand years). Substantial portions of Mars have experienced burial and subsequent exhumation (e.g., Malin and Edgett, 2001), and inverted channels are one landform that record this history. Preservation of discrete alluvial paleochannels is favored in depositional settings where channels are incised into weak materials, quickly infilled, and buried. On Mars, rapid burial of paleochannels by fines may have occurred via widespread volcanic ash-fall (e.g., Hynek et al., 2003) or pyroclastic deposit (e.g., Mandt et al., 2008), and marine (e.g., Baker et al., 1991) or lacustrine (e.g., Grant et al., 2008; Fassett and Head, 2008) deposition within basins. Like the terrestrial analogs in Utah discussed here, some Martian sinuous ridges appear to have undergone a complex evolution involving multiple phases (e.g., Fig. 3), and we present two examples that involved former burial and exhumation.

Light-toned layered materials have been recognized at a number of locations on Mars, particularly proximal to Valles Marineris (Malin and Edgett, 2000; Edgett, 2005) and sometimes in association with sinuous ridges (Weitz et al., 2010; LeDeit et al., 2010). One example is on the plains northwest of Juventae Chasma, where there are several sinuous ridge networks with varying planimetric pattern and different stratigraphic levels (Fig. 5; Williams et al., 2005; Weitz et al., 2010; Le Deit et al., 2010). This location is also notable because some of the fine-scale branching networks preserved in inverted relief have drainage densities (0.9–2.3 km^{-1}) among the highest observed on Mars and comparable to terrestrial fluvial systems of the same scale (Williams et al., 2005). Some of the sinuous ridges are partially buried by mesas, remnants of a formerly laterally extensive plains unit (Mangold et al., 2004). In other locations, examples of sinuous ridge networks are partially exhumed from a blanket of material. Figure 5C shows two sinuous ridges at different stratigraphic levels: a broadly sinuous ridge form trending roughly SW-NE that is stratigraphically beneath the dendritic branching ridge network that trends W-E. Sub-meter-resolution images of the sinuous ridges (e.g., Fig. 5B) show that they cap light-toned beds that appear to have

the same surface textures (e.g., polygonal fractures), color, and brightness variations observed in light-toned layered material elsewhere in the region (LeDeit et al., 2010; Weitz et al., 2010). Collectively, these observations show that changes in the fluvial environment (e.g., flow direction, flow regime) occurred during the Hesperian at this location.

Meridiani Planum is an excellent site to explore because there are exposures of horizontally bedded layered deposits. Hematite-bearing materials within the region first reported by Christensen et al. (2000) were of such interest that the Mars exploration rover *Opportunity* (MER-B) landed in Meridian Planum on 25 January 2004. Edgett (2005) conducted a photogeologic study of the region in which he identified four basic rock units and described an ~800 m stratigraphic section with the MER-B landing site located in the uppermost unit. Within these rock units, there are a range of preservation styles for valley networks, including inverted valleys, filled valleys, partially buried valleys, and exhumed negative-relief valleys (Edgett, 2005; Newsom et al., 2010). In Figure DR9 (see footnote 1), a dendritic network exhibits different surface expressions along its course. At the northern extreme, the low-relief trunk segment is laterally traceable to a series of layered ridges, indicating that the downstream portion of this system is buried (Fig. DR9B). In the midsection, the low-relief ridge transitions to a single negative-relief valley and further subdivides into a series of semiparallel, low-order segments defined by aligned pits at the southern extreme. Edgett (2005) speculated that the ridge-forming unit was once more extensive, and, therefore, this entire branching landform was formerly buried. A higher-resolution image of the northern portion (Fig. DR9D) shows that the light-toned, low-relief ridge is largely obscured by eolian bed forms and remnants of the former overburden; however, in isolated locations, the ridge exhibits a polygonal cracking pattern (that is occasionally contiguous with adjacent surface materials), which could be evidence for cementation. Alternatively, the former valley may have been filled with a resistant material that only affected the downstream reach. Whatever the cause, the downstream reach is more indurated than the middle and upstream sections; this lateral variation in resistance accounts for the different preservation styles. The presence of erosional surfaces on Mars, such as this one, indicates that there are unconformities in the Martian rock record.

Discussion: Meandering Streams

The four inverted paleochannel segments of the Ruby Ranch Member of the Cedar Mountain Formation (Fig. 10) are the preserved remnants of meandering streams with low sinuosity (Harris, 1980). The paleochannel segment with the highest sinuosity is located at this stop. The mechanics of meander formation are reasonably well understood from theory and empirical studies (Leopold and Wolman, 1957; Parker, 1976; van den Berg, 1995; Dade, 2000; Seminara, 2006). When flow enters a channel bend, a helical secondary current carves into the outer bank, resulting in a cutbank. Material mobilized in this process is transported by the secondary flow and can be deposited downstream on the next inner bend, creating a point bar. The net effect of these localized erosional and depositional zones is meander migration. Over time, meandering increases heliocoidal (screw-like) flow, resulting in greater meander amplitude. This increase in meander amplitude produces a series of subparallel, semiconcentric point-bar ridges (scroll bars) delineating the past positions of the river as it migrates laterally across the floodplain (Leopold et al., 1992; Knighton, 1998).

Bank cohesion has long been identified as a necessary component in the development of unconfined meandering channels (Howard, 2009). This factor results in meander channels with small aspect ratios (ratio of channel width to average depth 10–50). Bank stability generally is conferred either by cohesive, clay-rich sediment deposited from suspension or, more commonly, vegetation cover. In terrestrial settings, these two causative factors are interrelated. The effect of a protective vegetative cover has long been observed to promote more complete chemical weathering than on unvegetated slopes through longer residence times of weathered material, a wetter environment, and an acidic environment (as summarized, e.g., by Kennedy et al., 2006; Lowe, 2007). Meandering rivers in the terrestrial rock record are sparse until the advent of vascular plants (e.g., Cotter, 1978; Davies and Gibling, 2010, and references therein), although interpretation of the geologic record is complicated by the limited preservation of early rocks and their subsequent strong geochemical alteration.

Highly sinuous meandering channels have been found at a very few locations on Mars. Within Eberswalde crater, there is a multilobe distributary fan made up of sinuous, anabranching ridges, which is interpreted to be an exhumed delta that formed in the Late Noachian (Fig. 4; Malin and Edgett, 2003; Moore et al., 2003). Several of the sinuous ridges have meandering courses that record a complex history of migration, avulsion, and bifurcation (up to five orders of branching). Morphological studies reveal details regarding the sequence of events in delta development: Bhattacharya et al. (2005) identified 11 avulsion events, and Wood (2006) mapped six separate lobes within the delta complex. In the southeastern extreme of the landform, there are moderately sinuous channels (average sinuosity = 1.77) that display meander-bend migration and meander growth through lateral accretion (Wood, 2006). One loop-shaped ridge (labeled in Fig. 4) has concentric curvilinear lineations on the interior. Lateral shifting of this channel produced the scroll-bar ridges, a record of meander growth. Ultimately, during high-flow conditions, a chute produced a more direct path, resulting in a cutoff meander. The moderate sinuosity and chute cutoff morphology are consistent with bed load to mixed-load sediment-filled channels (Wood, 2006). The identification of evolving meander landforms provides concrete evidence that persistent flow occurred on Mars (Malin and Edgett, 2003). This location will be discussed again at stop 5.

Additional examples of meandering sinuous ridges are found near Juventae Chasma (fragmentary meanders in Fig. 5)

and in the Aeolis–Zephyria Plana region. In the Aeolis–Zephyria Plana region, some of these are multilevel landforms with a narrow, meandering ridge that is stacked atop a flat, broad mesa (Fig. 6; Burr et al., 2009). The flat mesa is interpreted to be a remnant floodplain that became indurated. Subsequently, sediments were deposited on the floodplain, and a meandering river flowed through the sediments. The last stage in the development of a multilevel sinuous ridge is erosion, which strips away the finer sediments, resulting in inversion of the late-stage meandering course and the earlier floodplain (see further details and a schematic in Burr et al., 2009). Semiconcentric, curved ridges on the flat mesa are interpreted to be scroll bars that record meander migration. Further discussion of the Aeolis–Zephyria Plana sinuous ridges is included at stop 5.

Factors that may promote bank cohesion on Mars to enable the generation of meanders in fluvial systems where vegetation apparently played no role may include (1) clay-rich sediment, (2) ice from permafrost, or (3) chemical cementation of floodplain deposits forming hardpans or duricrusts (Howard, 2009). The latter two mechanisms are straightforward to envision, but the former category has an interesting implication for Martian history. The generation of clays requires extensive chemical weathering. Clays have been detected in isolated locations on the Noachian highlands (e.g., Pelkey et al., 2007; Bishop et al., 2008; Buczkowski et al., 2008; Mustard et al., 2008), but the dominant spectral signature of the highlands is of basic igneous minerals, including olivine and pyroxene (e.g., Bandfield, 2002; Rogers and Christensen, 2007).

Return to Nine Mile Reservoir Road.

Mile 21.9 (0.9 incremental miles). Turn right on Nine Mile Reservoir Road. After ~2 miles, continue straight (south), as the road branches to the left (inverted paleochannels to the right).

Mile 24.7 (2.8 incremental miles). Stop 4. Channel A (Harris, 1980) in the Ruby Ranch Member (38°52′53″N, 110°17′6″W). The bases of the paleochannels have variable characteristics. At this location, channel A has a basal conglomerate with large limestone rip-up clasts (well displayed in the eastern outcrop; Fig. DR6B [see footnote 1]). In contrast, carbonate nodules are in the basal conglomerate at various sites in channel D (Fig. DR6C).

Road turns to east at 0.4 mile.

Mile 25.8 (1.1 incremental miles). Stop 5. Exhumed channels D and B (Harris, 1980) of the Ruby Ranch Member (38°52′15″N, 110°16′35″W). Walk east to the ridge and climb to the crest of the north-south–trending channel D. Walk 0.3 mile (500 m) north along channel D until it meets the east-west–trending channel B (Fig. DR10; 38°52′34″N, 110°16′16″W). From this vantage point, you can see that the two channels are at different topographic and stratigraphic levels. Channel segments did not form simultaneously. Note that one can be misled in orbital images or aerial photographs where it appears there is a junction between channels B and D, with the junction angle suggesting a former flow direction to the south. High-resolution topographic data have the potential to reveal that these two channel segments do not join at the same elevation.

Discussion: Paleoflow Reconstruction

Paleoflow reconstruction is useful in constraining the amount of water, duration of fluvial activity, and climatic conditions required to generate fluvial landforms. Studies of modern streams and laboratory flume experiments have led to equations for determining flow discharge (Knighton, 1998 and references therein). These flow equations can be subdivided into two categories, hydraulic relationships between sediment and flow parameters and geomorphic relationships among channel morphology, channel sediments, and discharge. The hydraulic or micro-approach (e.g., Jopling, 1966) provides estimates of short-term or instantaneous velocity or discharge conditions, as a result of local adjustment of hydraulic geometry around a mean or equilibrium channel condition. The geomorphic or macro-approach indicates the development of longer-term equilibrium or quasi-equilibrium conditions among catchment, channel, and flow parameters (e.g., Langbein and Leopold, 1964).

Recently, studies have demonstrated the validity of applying these hydrological models derived for modern terrestrial streams to inverted paleochannels on Earth (Maizels, 1983, 1987; Williams et al., 2009b), and by extension Martian sinuous ridges (Burr et al., 2010). Investigation of a gravel-capped inverted channel system in Oman demonstrated that relatively consistent results (well within one order of magnitude) were obtained from multiple models for such paleoflow parameters as flow depth, mean flow velocity, bed shear stress, bankfull or mean annual discharge, and peak discharge (Maizels, 1983, 1987). Williams et al. (2009b) conducted field-based measurements of channel slope, grain size, and sedimentary relations indicative of flow depth for two cemented paleochannels (channels B and D visible at this stop) in east-central Utah. Using 14 hydrologic models, they derived an envelope of plausible dominant discharge values (100–500 m^3/s) for these paleochannels that were consistent with field observations of paleoflow conditions. The range of paleoflow values can be narrowed when numeric models derived from comparable fluvial environments are used, but determining the former fluvial environment can be difficult, particularly in exhumed terrains where contextual clues have been erased. Thus, it is possible to reliably reconstruct the paleohydrologic conditions from preserved attributes of inverted channel systems.

A complication in applying flow models to Martian landforms is that the models must account for the lower gravitational acceleration on Mars. Gravity scaling of the micro-approach is straightforward (e.g., Komar, 1979). The limiting factors in applying the micro-approach stem from uncertainty in grain size (no ground-based observations of Martian sinuous ridges exist to date) and roughness coefficients (e.g., Manning coefficient, Darcy-Weisbach friction factor; Wilson et al., 2004; Kleinhans, 2005). However, gravity is not an explicit term in the empirical macro-approach, the favored method because it uses channel dimensions that are easily obtained from remotely sensed data. The lower Martian gravity would yield greater channel width, depth, and meander wavelength per unit discharge than on

Earth. The uncorrected macro-approach would overestimate the Martian discharge values by a factor of 1.61 (Irwin et al., 2008).

Assessing the paleohydrologic conditions for Martian sinuous ridges is a new area of research. We highlight two case studies. One of the first areas on Mars where inverted channels were identified is the Noachian-aged multilobe deltaic complex in Eberswalde crater (Fig. 4). Moore et al. (2003) used seven meander wavelength measurements to estimate a persistent flow magnitude of 700 m^3/s to form the deltaic deposit based on multiple empirical models that relate meander wavelength and discharge (macro-approach) as summarized in Knighton (1998). A wide range of minimum time estimates for this landform to accumulate have been reported, in part because of disagreement over the depositional environment and whether the landform developed over a continuous period or in discreet episodes. The formation period could have been very rapid: (1) several decades of active flow if it were associated with a few short episodes of constant heavy precipitation resulting from large impact events (e.g., Segura et al., 2002, 2008; although one should note shortcomings of this model for this site as discussed in Moore et al., 2003) or (2) less than a century if fan construction was entirely from river channels (i.e., without a standing body of water present) based on numerical models (Jerolmack et al., 2004). However, most workers interpret that the fan complex developed in a lacustrine setting, presumably under clement climate conditions that involved typical terrestrial precipitation rates. Lewis and Aharonson (2006) examined the stratigraphic configuration of the layers in high-resolution stereo images and found the shallow sloping layers consistent with a progradational delta. They proposed a development scenario involving a number of short-lived lacustrine episodes marked by a constantly rising lake level with a minimum formation time of several hundred years. Finally, assuming typical terrestrial sedimentation rates and avulsion periods for this site, the delta would have formed over thousands to millions of years (Moore et al., 2003; Bhattacharya et al., 2005).

The Aeolis–Zephyria Plana region hosts the largest concentration of sinuous ridges that are among the youngest such landforms on Mars (Fig. 6; Fig. DR11 [see footnote 1]). The sinuous ridges are found within the two western lobes of the equatorial Medusae Fossae Formation, an enigmatic and discontinuous deposit of fine-grained friable material (for discussion of the various proposed origins for the Medusae Fossae Formation, see Mandt et al., 2008, and references therein). Crater counts and observed superposition relationships among geologic units led to an age determination for the Medusae Fossae Formation of Amazonian (Tanaka, 1986), although recent work suggests portions of the deposit could be older, from the Late Hesperian (Kerber and Head, 2010). Burr et al. (2010) used terrestrially derived empirical relationships between river geometry and discharge, scaled for Martian gravity, to estimate paleodischarge for 16 reaches in 9 sinuous ridges in the Aeolis–Zephyria Plana. Their analysis, using measurements of channel width and wavelength, yielded discharge values between 10 and 1000 m^3/s; the largest of these estimates is comparable to paleodischarge estimates for some late-stage Noachian valley networks on Mars. Given the stratigraphic context of the sinuous ridges over an elevation range of 3500 m (Burr et al., 2009), fluvial activity must have occurred, likely episodically, over time scales of hundreds to thousands of years (Burr et al., 2010). The meandering morphology (Fig. 6; Fig. DR11 [see footnote 1]) and high sinuosity (>2) of some sinuous ridges in the Aeolis–Zephyria Plana indicate persistent flow over durations of several years. This work suggests that clement climate conditions at least regionally occurred at this equatorial location during the Late Hesperian to Early Amazonian time frame.

Retrace the route to Old State Route 24, a distance of ~4.5 miles. After traversing 4.3 miles, there is a junction in the road and both routes reach Old State Route 24; take the right branch.

Mile 30.1 (4.3 incremental miles). Turn right on State Route 24. There is a radio tower on the right after ~1.8 miles.

Mile 36.0 (5.9 incremental miles). Turn right on Old Hanksville Highway. Drive past Green River Municipal Airport.

Mile 38.5 (2.5 incremental miles). Turn left on County Road.

Mile 40.3 (1.8 incremental miles). Turn right on Lower San Rafael Road (County Road 1010; also known as Flint Trail). This is a well-maintained gravel road, suitable for most vehicles.

Mile 43.0 (2.7 incremental miles). Cross Fivemile Wash.

Mile 44.8 (1.8 incremental miles). Cross Ninemile Wash.

Mile 46.5 (1.7 incremental miles). Stop 6. Exhumed paleochannel segment B in the Ruby Ranch Member (38°52′50″N, 110°12′25″W). Road cut through single thread channel of Cedar Mountain Formation. Park your vehicle well off the road and walk west to the outcrop. This stop affords the opportunity to examine the basal contact of channel "D" with underlying mud deposits (Fig. DR6A).

Climb to the top of the outcrop and look to the northeast, where fault offsets are evident in the fracture zone located east of the road. Faults within the Cedar Mountain Formation are concentrated in the eastern portion of the study region (Figs. 1 and 10A) and consistently strike west-northwest to east-southeast, regardless of the local channel axis orientation. These faults have normal offsets of up to a few tens of meters and can be traced several kilometers along strike to the Salt Wash fault system to the east (Williams and Hackman, 1971; Doelling, 2002). The extension fractures in these inverted channels most likely formed simultaneously with the local faults in response to vertical overburden stress (Lorenz et al., 2006). Faults were probably active during early Tertiary and Quaternary time, but displacement during middle Cretaceous time cannot be excluded (Shipton et al., 2004).

If time permits, walk along this horseshoe meander segment, which is ~1.9 miles (~3 km) in length. Note variations in preservation style (discussed next) at different sections of the channel.

Discussion: Preservation Variations

Differences in preservation style of inverted channels are important to recognize because these characteristics may be important criteria for identifying inverted channels on Mars.

Broadly speaking, terrestrial inverted channels typically are flat-topped, in contrast to a rounded or sharp-crested profile that can be found in other ridge landforms, such as eskers. However, the preserved channel deposits have subtle variations in morphology related to their depositional setting along course. As can be seen at this site, point-bar deposits, found on the inner channel bend, have irregular meter-scale undulations on the surface and rounded margins. Channel-fill materials have flat surfaces, uniform widths, and vertical cliff margins (Harris, 1980).

These inverted paleochannels have relatively uniform width along course, as can be seen in aerial photographs. Variations in width values reflect incomplete preservation, destruction of the paleochannels by subsequent erosion, and the type of channel deposit, with regions that are exclusively channel-fill deposits coinciding with greater widths (Williams et al., 2009b). These along-course changes in width are important to recognize because channel width is an input variable in some macroscale equations for determining paleodischarge. There is the potential to underestimate channel width in regions of poor preservation or overestimate channel width, particularly in regions of channel migration. Williams et al. (2009b) recommended adopting the third quartile of measured maximum channel widths as a representative value of the former active channel width.

The paleochannels within the Cedar Mountain Formation are discontinuously preserved in discrete sections. The former lateral continuity can be inferred assuming that in-line channel sections were once connected. Erosion of the underlying mudstone leads to undermining of the channel (cap rock), which breaks down into blocks that are transported downslope by mass wasting. Where the cap rock has been removed, the underlying mudstone develops a rounded crest that is a trace of the former channel course (Fig. DR12 [see footnote 1]).

Some meandering ridges in the Aeolis–Zephyria Plana are fragmentary in nature, extending only a few tens of meters in length, and showing only partial preservation of the former flow course. Lateral variations in induration result in discontinuous sinuous ridges. For example, wind erosion has sculpted a former sinuous ridge into a series of aligned knobs that mark the former flow path (Fig. DR11 [see footnote 1]).

Background: Salt Wash Member Paleochannels

Paleochannels within the Salt Wash Member of the Morrison Formation are located in the Lower San Rafael Desert (Fig. 12). These channel-fill deposits are composed of relatively homogeneous quartz sand grains with occasional pebble-lag deposits that form beautiful white sandstone (Fig. 13). Large-scale trough cross-beds are evident on the paleochannel surfaces, indicating paleoflow to the northeast. The medium- to coarse-grained quartz sandstone is bound primarily by silica overgrowth cements with minor calcite cement (Fig. DR13; Williams et al., 2009a). The site has numerous superimposed paleochannel segments with different azimuths, reflecting variations in the streamflow patterns over time. Ultimately, the result of this migration is a preserved, time-transgressive surface of vertically stacked paleochannels (Figs. 12B and 12C); the superposition of inverted channels evident at this site is analogous to that observed in the deltaic complex at Eberswalde crater (Fig. 4).

Pass Horse Bend Reservoir after ~2 miles. Following heavy rains, the road may be impassable.

Mile 51.9 (5.4 incremental miles). Stop 7. Inverted Paleochannels in the Salt Wash Member (38°48′32.98″N, 110°13′36.65″W). At this location, there is a small metal grave marker to commemorate the life of Charles W. Watterson Jr., an employee of the Emery County Road Department, who was tragically murdered while operating a road grader. Scott Merrill pled "no contest" to aggravated murder in exchange for a life sentence, and he tried unsuccessfully to withdraw his plea in a case decided by the Utah Supreme Court in 2005. Court documents indicate that Mr. Merrill was mentally unstable (schizophrenic, or possibly bipolar) and believed that he was acting according to God's will.

The quartz sandstone that makes up these inverted channels differs from other locales visited so far in that it lacks any coatings or desert varnish. Therefore, the channel-fill deposits and sedimentary structures are readily visible and quite striking at this site. Lateral continuity of individual channels is limited to less than a few hundred meters. If time permits, you can explore the area and walk along the channels to see superposition relationships between different time-transgressive channels. Inverted channels extend to the northeast about ~1.9 miles (~3 km), where they terminate in a cliff face. Figure DR14 (see footnote 1) illustrates the underlying muddy floodplain deposits exposed beneath the paleochannels cap rock at this cliff.

Discussion: Cementation Mechanisms

Petrographic examination of lithified channel sediments from sites 2, 6, and 7 shows evidence of cementation prior to significant burial, which inhibited the detrital grains from completely compacting or having significant grain-to-grain pressure solution (Williams et al., 2009a). In the Utah study area (Fig. 1), cement composition varied by region. Early diagenetic waters formed coarse crystalline ("sparry") calcite cements within some inverted channels in the western channel systems (not presented here; Williams et al., 2009a), while complete silica (mega-quartz and chert) cementation occurred in the central system (paleochannels in the Cedar Mountain Formation), and a mixture of both calcite and silica cements formed in the northwestern and southeastern systems (Brushy Basin and Lower San Rafael Desert paleochannels). Differences in cement mineralogy may reflect either a variation in the age of the early cements or changes in groundwater chemistry (i.e., a difference in the composition of the rocks through which the diagenetic waters passed) prior to cementation. Cementation of these channel deposits may have occurred via evaporation of groundwater that concentrated water-soluble minerals at the surface in abandoned streams or during the dry season in ephemeral streams, leading to an indurated fluvial deposit.

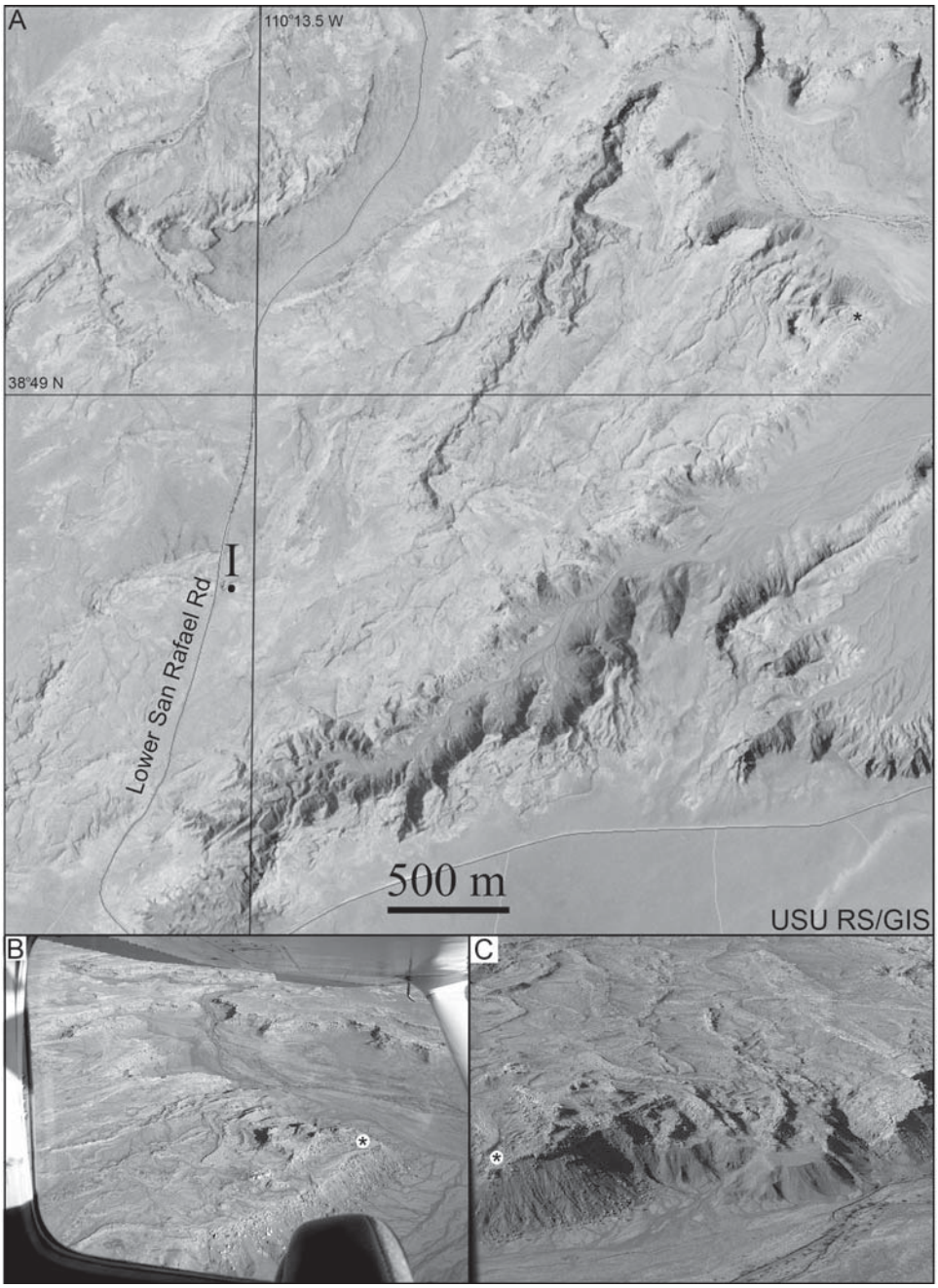

Figure 12. (A) Aerial photomosaic (1 m/pixel, acquired in 2006) of inverted fluvial sediments in the Late Jurassic Salt Wash Member of the Morrison Formation located in the Lower San Rafael Desert. See box marked 7 in Figure 1 for site location. Thin sections were made from samples collected at location marked "I" and are illustrated in Figure DR13 (see text footnote 1). Asterisk marks common location in all panels. (B–C) Aerial photographs showing the overlapping relationships among the inverted channels (B, view to the north; C, view to the southwest). Note that 500 m is approximately equivalent to 0.3 mile. Panel A is an annotated image from Virtual Utah (http://earth.gis.usu.edu/utah), Remote Sensing and GIS Laboratory, Utah State University, Logan. Aerial photos are by R. Williams.

For these inverted channels, early diagenetic cementation of the channel sediments in the near-surface environment allowed them to be preserved by differential erosion. Additional terrestrial cemented inverted channels at sites around the world are under investigation. Results to date, although limited, suggest that early aqueous diagenetic processes may be a key phase in the development of cemented inverted channels on Earth, and by extension, on Mars (Williams et al., 2009a).

Cementation of fluvial deposits on Mars could occur via a number of mechanisms. Near-surface cementation, analogous to what occurred at these analog sites, is a likely form of induration on Mars (Pain et al., 2007). In this case, cementation would have occurred associated with or shortly after the period of fluvial activity, and a separate clement period is not required. Other scenarios for cement generation include degassing (discharging groundwaters that contain dissolved gasses such as CO_2), fluid mixing during regional groundwater flow, cooling of hydrothermal waters (e.g., Newsom et al., 2001; Rathbun and Squyres, 2002), or the precipitation of salts through sublimation of an icy saline regolith (e.g., Wentworth et al., 2005). Further discussion of these mechanisms may be found in Pain et al. (2007) and references therein.

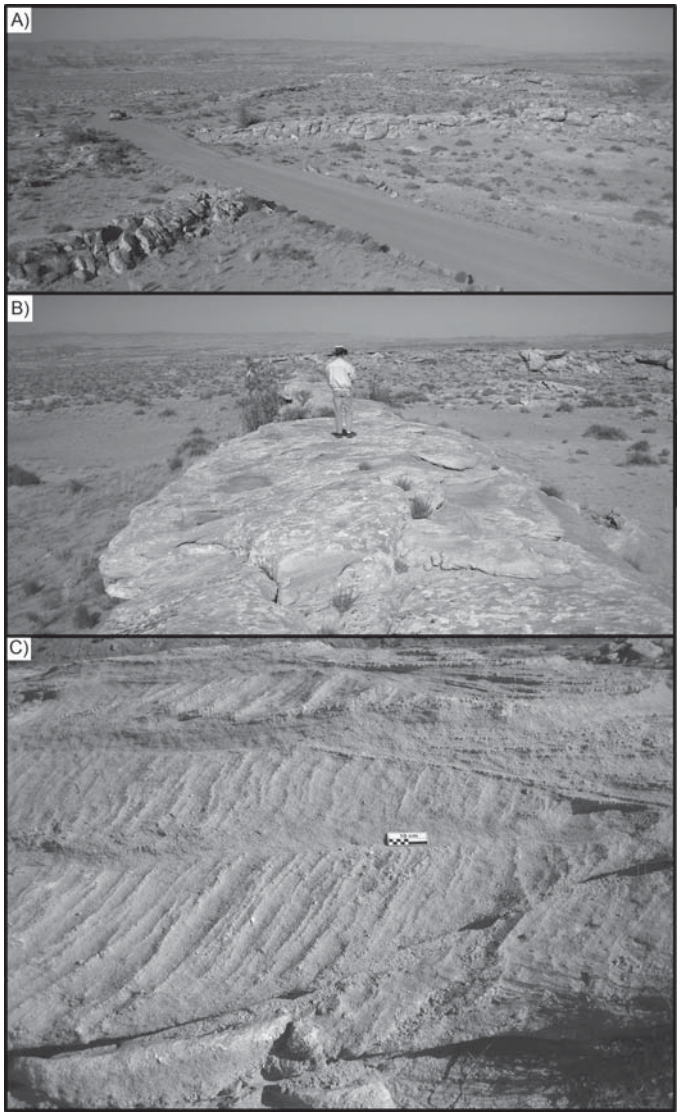

Figure 13. (A) Overview of multistoried inverted channel complexes in the Lower San Rafael Desert. Car on road gives a sense of scale. Photo by J. Zimbelman. (B) Inverted paleochannels (~3 m width) at this location have low relief, uniform width, and lateral continuity of a few hundred meters. Photo by J. Zimbelman. (C) Planar and trough cross-beds are evident on the surface. Scale bar is 10 cm. Photo by R. Williams.

CONCLUDING REMARKS

The three inverted paleochannel sites in east-central Utah discussed in this work differ in scale, age, and fluvial environment, but all are bound by cements that formed in the near-surface environment. Ultimately, these channel sediments were buried to 2400 m before Laramide uplift and differential erosion of the surrounding units exposed the channel-fill deposits. Terrestrial analog studies of inverted channels are helping to elucidate the diagnostic criteria for identifying these landforms, variations in formation scenarios that develop inverted channels, the environmental conditions associated with cementation, and the applicability of paleohydrological models to inverted fluvial landforms. Close-up and three-dimensional views of terrestrial inverted paleochannels are critical background for interpreting observations from potential future surface exploration of Mars. For example, there are inferred inverted channels within the landing ellipse at Gale Crater for the Mars Science Lander (MSL), which is scheduled to launch in fall 2011 (Anderson and Bell, 2010).

APPENDIX A

Lithostratigraphic Units

This section provides a general description of the lithostratigraphic units associated with the exhumed paleochannels found in the region of interest (Fig. 2; Doelling, 2002). Paleochannels in the road log are within the Ruby Ranch Member of the Cedar Mountain Formation and both members of the Morrison Formation.

The skyline to the west of Green River is dominated by the dramatic, northeast-trending San Rafael Swell, an asymmetric anticline that exposes older Triassic and Permian rocks than those located in the region of interest. The eastern limb, known as the San Rafael Reef, is characterized by flatiron exposures of dipping strata. Near the base, there are dark triangular wedges of the Carmel Formation, whereas the prominent light-toned flatirons include the Navajo, Kayenta, and Wingate Sandstones (listed down-section) of the Early Jurassic Glen Canyon Group.

Carmel Formation

The Carmel Formation includes siltstone, shale, and sandstone that were deposited in shallow-marine and mud-flat environments during the Middle Jurassic (Doelling, 2002; Hintze and Kowallis, 2009).

Entrada Formation

Several facies are reflected in the Entrada Formation, which is most famous for the red sandstone that commonly erodes into arches as in Arches National Park. Brown hoodoos are present at nearby Goblin Valley State Park, and the formation is marked by brown siltstone in layered cliffs within the study area (Hintze and Kowallis, 2009). This unit was deposited in tidal mud flats, beaches, and nearshore sand dunes (Peterson, 1988).

Curtis Formation

Marine sediments from the Sundance or Zuni Sea, which includes green shale and glauconitic sandstone, comprise the Curtis Formation (Doelling, 2002; Hintze and Kowallis, 2009).

Summerville Formation

Thin-bedded red siltstone, shale ,and gypsum may have been deposited in a tidal-flat or lagoonal setting as the Sundance or Zuni Sea retreated (Peterson, 1972).

Morrison Formation

Famous for its dinosaur fossils, the Morrison Formation was originally described in 1894 by C.W. Cross in Morrison, Colorado (Cross, 1894). The Morrison Formation consists of moderate- to thin-bedded shale and siltstone with intermittent lenses of sandstone and conglomerate (Stokes, 1944, 1961; Derr, 1974). Reconstruction of the climatic and hydrologic conditions in the Morrison depositional basin indicates that a dry climate prevailed during the Late Jurassic. Most of the moisture that reached the Morrison depositional basin originated from extrabasinal uplands to the west (Turner and Peterson, 2004). The fluvial environment within the basin fluctuated with the seasons. A high water table during the wet season produced streams, wetlands, and lakes. During dry seasons, lakes would shrink or evaporate, and streams would flow intermittently or transition to substream flow. Rapid facies changes occur over small lateral distances. Within the region of interest, two members of the Morrison Formation, the Salt Wash and Brushy Basin Members, have examples of exhumed paleochannels.

Tidwell Member. The thin (<15 m), basal member of the Morrison Formation consists of calcareous siltstone interbedded with a fine-grained sandstone and limestone. Locally, there is a thick (5 m) gypsum bed at the base (Doelling, 2002). These rocks are interpreted to be associated with a changing environment upward through the section from sabkha to floodplain and then lacustrine.

Salt Wash Member. The Salt Wash Member is the basal member of the Late Jurassic Morrison Formation and is found in parts of Utah, Colorado, Arizona, and New Mexico. Deposited by streams, this unit includes lenticular beds of cross-laminated sandstone irregularly interbedded with mudstone, siltstone, claystone, and horizontally laminated sandstone (Mullens and Freeman, 1957). The sandstone has been a major source of uranium on the Colorado Plateau.

Brushy Basin Member. In this region, the Brushy Basin Member reaches nearly 100 m in thickness. It was formed mainly by fluvial sedimentation that produced extensive floodplains, and lake deposits (Stokes, 1944) under a semiarid climate (Turner and Fishman, 1991; Currie, 1998). Composed primarily of claystone, mudstone, siltstone, and shale in an array of colors (reds, purples, grays, and gray greens), it commonly weathers to a popcorn-like surface (Trimble and Doelling, 1978). Multicolored badlands and rounded hills are common surface expressions of this unit. Within this unit, there are discontinuous medium- to fine-grained quartz sandstone channel segments bound by calcite and silica cements. The largest sandstone lenses often have conglomerate at the base. Prior to erosion, the channel segments were entirely surrounded by siltstones and shales; green and yellow-brown shale subjacent to the channel base formed in a reducing environment at the channel-floodplain interface. In addition, discontinuous patches of lacustrine limestone associated with local lakes are present (Craig et al., 1955).

Cedar Mountain Formation

Sediments of the Cedar Mountain Formation were originally deposited in rivers, lakes, and floodplain settings. The Cedar Mountain Formation is principally located in eastern Utah, and two members of the unit are present within the region of interest. Inverted paleochannels have been identified in the Ruby Ranch Member.

Buckhorn Conglomerate Member. The base of the Cedar Mountain Formation is defined by the discontinuous Buckhorn Conglomerate Member (Stokes, 1952), with thickest exposures (9 m) located to the north near the San Rafael Swell (Doelling, 2002). Near this site, the Buckhorn Conglomerate is composed of sand- and pebble-size fragments of mainly chert and quartzite.

Ruby Ranch Member. The Ruby Ranch Member (Kirkland et al., 1999; Kirkland and Madsen, 2007) is dominantly bedded mudstone bearing abundant carbonate nodules with fluvial sandstone lenses representing ribbon sandstones that formed on the coastal plain between the rising Sevier orogenic belt to the west and the rising Cretaceous Western Interior Seaway to the east. This ~50-m-thick member is composed principally of bentonitic siltstone, shale, and mudstone, with minor sandstone and limestone (Trimble and Doelling, 1978). Where unprotected by a cap rock, the shale portion of this member forms badlands or rounded hills. Many of the conglomeratic sandstone lenses within the Ruby Ranch Member are exposed at the surface, as erosion has removed much of the softer, encasing floodplain shale and siltstone. Weathering and erosion of the underlying shales have led to cliff-face spalling of the channel margins.

Dakota Sandstone

The Dakota Sandstone is the basal deposit of the transgressive Cretaceous seaway (Lawyer, 1972; Hintze and Kowallis, 2009). First named in 1862 for deposits in the Midwest (Meek and Hayden, 1862), within the region of interest it is a thin (<10 m), discontinuous light-yellow sandstone with very limited exposure. In this region, the Dakota Sandstone fills shallow scours and appears to be fluvial (Trimble and Doelling, 1978).

Mancos Shale

The Mancos Shale is an extensive (900 m thick) marine deposit that formed in the Late Cretaceous interior seaway. The unit is primarily a gray mudstone, which accumulated in offshore and open-marine environments, with interfingering sandstones (often from fluvial sources) and calcareous shale (e.g., Hettinger and Kirschbaum, 2002). The basal portion ranges from clayey, fissile shale to a massive silty mudstone.

APPENDIX B

Alternate Route

This abridged road log is suitable for all vehicles and includes stops at inverted paleochannels from all three lithostratigraphic units. The route is subdivided into two legs. For consistency, stops are numbered as they are in the road log. See road log for stop details.

Leg 1: Exhumed Paleochannels in the Brushy Basin Member of the Morrison Formation

(All sites in this section are on paved roads.)

Mile 1.0 (0.0 incremental miles). Begin at U.S. Post Office located at the corner of Clark and Main Streets in Green River. Zero odometer. Head west on Main Street and enter Interstate 70 (I-70) westbound.

Mile 12.0 (12.0 incremental miles). Stop 1. Road cut through Brushy Basin Member paleochannels (38°55′44″N, 110°21′50″W).

Proceed east on I-70 to the next exit for Route 24. Turn right at end of exit ramp. The road is paved for only a short distance, and at the transition to a graded dirt road, there is ample room to park. It is a short walk <0.3 mile (<500 m) west to stop 2.

Mile 13.1 (1.0 incremental miles). Stop 2. Additional paleochannel examples from the Brushy Basin Member (38°55′37.40″N, 110°22′43.96″W).

End of leg 1.

Leg 2: Exhumed Paleochannels in the Cedar Mountain and Morrison Formations

(The majority of this route is on a well-maintained graded dirt road. After recent heavy rainfall, the road may be muddy in spots and impassable at Horse Bench Reservoir.)

Mile 0.0. Begin at U.S. Post Office located at the corner of Clark Street and Main Street in Green River. Zero odometer. Head one block west on Main Street and turn left on Long Street, which will dead end at Green River Avenue. Turn Left.

Mile 0.5 (0.5 incremental miles). Turn right on Airport Road and cross the train tracks.

Mile 2.9 (2.4 incremental miles). Turn left on Lower San Rafael Road (County Road 1010; also known as Flint Trail), a graded dirt road.

Mile 5.6 (2.7 incremental miles). Cross Fivemile Wash.

Mile 7.4 (1.8 incremental miles). Cross Ninemile Wash.

Mile 9.0 (1.6 incremental miles). Stop 6. Segment B (Harris, 1980) (38°52′50.08″N, 110°12′25.20″W).

Mile 11.2 (2.2 incremental miles). Horse Bench Reservoir on right.

Mile 14.4 (3.2 incremental miles). Stop 7. Exhumed paleochannels in the Salt Wash Member of the Morrison Formation (38°48′32.98″N, 110°13′36.65″W).

End of leg 2.

ACKNOWLEDGMENTS

The authors are grateful to Brian S. Currie, Department of Geology, Miami University (Ohio), for introducing us to the Ruby Ranch paleochannels and Jamie Laws for information on Charles W. Watterson Jr. We thank James I. Kirkland, State Paleontologist (Utah Geological Survey [UGS]), for assistance with the stratigraphy and environmental interpretation of the Cedar Mountain Formation. We appreciate the contributions of James Parker, Liz Paton, Sharon Wakefield, and Sharon Hamre of the UGS, who drafted figures. We thank David E. Tabet, Michael D. Hylland, Ken Page, and an anonymous party for their thorough reviews of this manuscript. This work was supported through National Aeronautics and Space Administration (NASA) Mars Fundamental Research grant NNX06AB21G awarded to R.M.E. Williams. This is Planetary Science Institute contribution 484.

REFERENCES CITED

Anderson, R.B., and Bell, J.F., 2010, Geologic mapping and characterization of Gale Crater and implications for its potential as a Mars Science Laboratory landing site: Mars, v. 5, p. 76–128.

Armstrong, J.C., and Leovy, C.B., 2005, Long term wind erosion on Mars: Icarus, v. 176, p. 57–74, doi:10.1016/j.icarus.2005.01.005.

Baker, V.R., 1982, The Channels of Mars: Austin, Texas, University of Texas Press, 198 p.

Baker, V.R., and Partridge, J.B., 1986, Small Martian valleys: Pristine and degraded morphology: Journal of Geophysical Research, v. 91, no. B3, p. 3561–3572, doi:10.1029/JB091iB03p03561.

Baker, V.R., Strom, R.G., Gulick, V.C., Kargel, J.S., Komatsu, G., and Kale, V.S., 1991, Ancient oceans, ice sheets and the hydrological cycle on Mars: Nature, v. 352, p. 589–594, doi:10.1038/352589a0.

Bandfield, J.L., 2002, Global mineral distributions on Mars: Journal of Geophysical Research, v. 107, p. 5042, doi:10.1029/2001JE001510.

Bandfield, J.L., Glotch, T.D., and Christensen, P.R., 2003, Spectroscopic identification of carbonate minerals in the Martian dust: Science, v. 301, p. 1084–1087, doi:10.1126/science.1088054.

Bhattacharya, J.P., Payenberg, T.H.D., Lang, S.C., and Bourke, M., 2005, Dynamic river channels suggest a long lived Noachian crater lake on Mars: Geophysical Research Letters, v. 32, L10201, doi:10.1029/2005GL022747.

Bibring, J.P., Gendrin, A., Gondet, G., Poulet, F., Berthe, M., Soufflot, A., Arvidson, R., Mangold, N., Mustard, J., Drossart, P., and OMEGA Team, 2005, Mars surface diversity as revealed by the *OMEGA/Mars Express* observations: Science, v. 307, p. 1576–1581, doi: 10.1126/science.1108806.

Bibring, J.P., Langevin, Y., Mustard, J.F., Poulet, F., Arvidson, R., Gendrin, A., Gondet, B., Mangold, N., Pinet, P., Forget, F., and OMEGA Team, 2006, Global mineralogical and aqueous Mars history derived from *OMEGA/Mars Express* data: Science, v. 312, p. 400–404, doi:10.1126/science.1122659.

Bishop, J.L., Noe Dobrea, E., McKeown, et al., 2008, Phyllosilicate diversity and past aqueous activity revealed at Mawrth Vallis, Mars: Science, v. 321, p. 830–833, doi:10.1126/science.1159699.

Buczkowski, D.L., Murchie, S.L., Seelos, F.P., Malaret, E., Hash, C., and CRISM Team, 2008, CRISM Analyses of Argyre Basin [abs.]: Houston, Texas, Lunar and Planetary Institute, Lunar and Planetary Institute Conference XXXIX, abstract 1030 (CD-ROM).

Burr, D.M., Enga, M.T., Williams, R.M.E., Zimbelman, J.R., Howard, A.D., and Brennand, T.A., 2009, Pervasive aqueous paleoflow features in the Aeolis/Zephyria Plana region, Mars: Icarus, v. 200, p. 52–76, doi:10.1016/j.icarus.2008.10.014.

Burr, D.M., Chojnacki, M., and Williams, R.M.E., 2010, Inverted fluvial features in the Aeolis/Zephyria Plana region, Mars: Formation mechanism and initial paleodischarge estimates: Journal of Geophysical Research, v. 115, E07011, doi:10.1029/2009JE003496.

Cabrol, N.A., and Grin, E.A., 2010, Lakes on Mars: Oxford, Elsevier, 550 p.

Carr, M.H., 1989, Recharge of the early atmosphere of Mars by impact-induced release of CO_2: Icarus, v. 79, p. 311–327, doi:10.1016/0019-1035(89)90080-8.

Carr, M.H., 1996, Water on Mars: New York, Oxford University Press, 119 p.

Carr, M.H., and Clow, G.D., 1981, Martian channels and valleys: Their characteristics, distribution, and age: Icarus, v. 48, p. 91–117, doi:10.1016/0019-1035(81)90156-1.

Christensen, P.R., Bandfield, J.L., Clark, R.N., Edgett, K.S., Hamilton, V.E., Hoefen, T., Kieffer, H.H., Kuzmin, R.O., Lane, M.D., Malin, M.C., Morris, R.V., Pearl, J.C., Pearson, R., Roush, T.L., Ruff, S.W., and Smith, M.D., 2000, Detection of crystalline hematite mineralization on Mars by the Ther-

mal Emission Spectrometer: Evidence for near-surface water: Journal of Geophysical Research, v. 105, no. E4, p. 9623–9642, doi:10.1029/1999JE001093.

Cotter, E., 1978, The evolution of fluvial style, with special reference to the central Appalachian Paleozoic, *in* Miall, A.D., ed., Fluvial Sedimentology: Canadian Society of Petroleum Geologists Memoir 5, p. 361–383.

Craddock, R.A., and Maxwell, T.A., 1993, Geomorphic evolution of the Martian highlands through ancient fluvial processes: Journal of Geophysical Research, v. 98, p. 3453–3468, doi:10.1029/92JE02508.

Craddock, R.A., Maxwell, T.A., and Howard, A.D., 1997, Crater morphometry and modification in the Sinus Sabaeus and Margaritifer Sinus regions of Mars: Journal of Geophysical Research, v. 102, p. 13,321–13,340, doi:10.1029/97JE01084.

Craig, L.C., Holmes, C.N., Cadigan, R.A., Freeman, V.L., Mullens, T., and Weir, G.W., 1955, Stratigraphy of the Morrison and Related Formations, Colorado Plateau Region, A Preliminary Report: U.S. Geological Survey Bulletin 1009-E, p. 125–168.

Cross, W.C., 1894, Description of the Pikes Peak Sheet: U.S. Geological Survey Atlas, Folio 7, 5 p.

Currie, B.S., 1998, Upper Jurassic–Lower Cretaceous Morrison and Cedar Mountain Formation, NE Utah–NW Colorado: Relationships between nonmarine deposition and early Cordilleran foreland-basin development: Journal of Sedimentary Research, v. 68, p. 632–652.

Dade, W.B., 2000, Grain size, sediment transport and alluvial channel pattern: Geomorphology, v. 35, p. 119–126, doi:10.1016/S0169-555X(00)00030-1.

Davies, N.S., and Gibling, M.R., 2010, Paleozoic vegetation and the Siluro-Devonian rise of fluvial lateral accretion sets: Geology, v. 38, p. 51–54, doi:10.1130/G30443.1.

Derr, M.E., 1974, Sedimentary structure and depositional environment of paleochannels in the Jurassic Morrison Formation near Green River, Utah: Brigham Young University Geology Studies, v. 21, p. 3–39.

Doelling, H.H., 2002, Interim Geologic Map of the San Rafael Desert 30′ × 60′ Quadrangle, Emery and Grand Counties, Utah: Utah Geological Survey Open-File Report 404, 20 p., 2 plates, scale 1:100,000.

Dundas, C.M., McEwen, A.S., Diniega, S., and Byrne, S., 2010, New and recent gully activity on Mars as seen by HiRISE: Geophysical Research Letters, v. 37, L07202, doi:10.1029/2009GL041351.

Edgett, K.S., 2005, The sedimentary rocks of Sinus Meridiani: Five key observations from data acquired by the *Mars Global Surveyor* and *Mars Odyssey* orbiters: Mars, v. 1, p. 5–58, doi:10.1555/mars.2005.0002.

Ehlmann, B.L., Mustard, J.F., Murchie, S.L., Poulet, F., Bishop, J.L., Brown, A.J., Calvin, W.M., Clark, R.N., Des Marais, D.J., Milliken, R.E., Roach, L.H., Roush, T.L., Swayze, G.A., and Wray, J.J., 2008, Orbital identification of carbonate-bearing rocks on Mars: Science, v. 322, doi:10.1126/science.1164759.

Fassett, C.I., and Head, J.W.I., 2008, Valley network-fed, open-basin lakes on Mars: Distribution and implications for Noachian surface and subsurface hydrology: Icarus, v. 198, p. 37–56, doi:10.1016/j.icarus.2008.06.016.

Glotch, T.D., Bandfield, J.L., Christensen, P.R., Calvin, W.M., McLennan, S.M., Clark, B.C., Rogers, A.D., and Squyres, S.W., 2006, Mineralogy of the light-toned outcrop at Meridiani Planum as seen by the Miniature Thermal Emission Spectrometer and implications for its formation: Journal of Geophysical Research, v. 111, doi:10.1029/2005JE002672.

Golombek, M.P., and Bridges, N.T., 2000, Erosion rates on Mars and implications for climate change—Constraints from the *Pathfinder* landing site: Journal of Geophysical Research, v. 105, p. 1841–1854, doi:10.1029/1999JE001043.

Golombek, M.P., Grant, J.A., Crumpler, L.S., Greeley, R., Arvidson, R.E., Bell, J.F., Weitz, C.M., Sullivan, R., Christensen, P.R., Soderblom, L.A., and Squyres, S.W., 2006, Erosion rates at the Mars exploration rover landing sites and long-term climate change on Mars: Journal of Geophysical Research, v. 111, doi:10.1029/2006JE002754.

Grant, J.A., Irwin, R.P., III, Grotzinger, J.P., Milliken, R.E., Tornabene, L.L., McEwen, A.S., Weitz, C.M., Squyres, S.W., Glotch, T.D., and Thomson, B.J., 2008, HiRISE imaging of impact megabreccia and sub-meter aqueous strata in Holden Crater, Mars: Geology, v. 36, p. 195–198, doi:10.1130/G24340A.1.

Haberle, R.M., McKay, C.P., Schaeffer, J., Cabrol, N.A., Grin, E.A., Zent, A.P., and Quinn, R.M., 2001, On the possibility of liquid water on present day Mars: Journal of Geophysical Research, v. 106, p. 23,317–23,326, doi:10.1029/2000JE001360.

Halevy, I., Zuber, M.T., and Schrag, D.G., 2007, A sulfur dioxide climate feedback on early Mars: Science, v. 318, no. 5858, p. 1903–1907, doi:10.1126/science.1147039.

Harms, J.C., and Fahnestock, R.K., 1965, Stratification, bed forms, and flow phenomena (with an example for the Rio Grande): Society of Economic Paleontology Mineral Special Publication 12, p. 84–115.

Harris, D.R., 1980, Exhumed paleochannels in the Lower Cretaceous Cedar Mountain Formation near Green River: Brigham Young University Geology Studies, v. 27, p. 51–66.

Harrison, K.P., and Grimm, R.E., 2005, Groundwater-controlled valley networks and the decline of surface runoff on early Mars: Journal of Geophysical Research, v. 110, 17 p., doi:10.1029/2005JE002455.

Harrison, T.N., Malin, M.C., and Edgett, K.S., 2009, Present-day gully activity observed by the *Mars Reconnaissance Orbiter* (MRO) Context Camera (CTX) [abs.], *in* 41st Division of Planetary Sciences of the American Astronomical Society Annual Meeting Abstracts: Fajardo, Puerto Rico, Division of Planetary Science, v. 41, no. 3, Abstract # 57.03.

Hettinger, R.D., and Kirschbaum, M.A., 2002, Stratigraphy of the Upper Cretaceous Mancos Shale (Upper Part) and Mesaverde Group in the Southern Part of the Uinta and Piceance Basins, Utah and Colorado: U.S. Geological Survey Pamphlet to accompany Geologic Investigations Series I-2764, 21 p.

Hintze, L.F., and Kowallis, B.J., 2009, Geologic History of Utah: Brigham Young University Geology Studies Special Publication 9, 225 p.

Hintze, L.F., Willis, G.C., Laes, D.Y.M., Sprinkle, D.A., and Brown, K.D., 2000, Digital Geologic Map of Utah: Utah Geological Survey Map 179DM, scale 1:500,000.

Howard, A.D., 1981, Etched plains and braided ridges of the south polar region of Mars: Features produced by basal melting of ground ice?: NASA Technical Memorandum 84211, p. 286–288.

Howard, A.D., 2009, How to make a meandering river: Proceedings of the National Academy of Sciences of the United States of America, v. 106, no. 41, p. 17,245–17,246, doi:10.1073/pnas.0910005106.

Howard, A.D., Moore, J.M., and Irwin, R.P., III, 2005, An intense terminal epoch of widespread fluvial activity on early Mars: 1. Valley network incision and associated deposits: Journal of Geophysical Research, v. 110, no. E12, doi:10.1029/2005JE002459.

Hunt, C.B., 1969, Geologic history of the Colorado River: U.S. Geological Survey Professional Paper 669-C, p. 59–130.

Hynek, B.M., and Phillips, R.J., 2001, Evidence for extensive denudation of the Martian highlands: Geological Society of America Bulletin, v. 29, p. 407–410.

Hynek, B.M., Phillips, R.J., and Arvidson, R.E., 2003, Explosive volcanism in the Tharsis region: Global evidence in the Martian geologic record: Journal of Geophysical Research, v. 108, no. E9, 5111, doi:10.1029/2003JE002062.

Hynek, B.M., Breach, M., and Hoke, M.R.T., 2010, Updated global map of Martian valley networks and implications for climate and hydrologic processes: Journal of Geophysical Research, v. 115, no. E09008.

Irwin, R.P., III, Howard, A.D., and Craddock, R.A., 2008, Fluvial valley networks on Mars, *in* Rice, S., Roy, A., and Rhoads, B., eds., River Confluences, Tributaries, and the Fluvial Network: West Sussex, UK, John Wiley and Sons, p. 409–430.

Jerolmack, D.J., Mohrig, D., Zuber, M.T., and Bryne, S., 2004, A minimum time for the formation of Holden Northeast fan, Mars: Geophysical Research Letters, v. 31, 5 p., doi:10.1029/2004GL021326.

Johnson, S.J., Mishna, M.A., Grove, T.L., and Zuber, M.T., 2008, Sulfur-induced greenhouse warming on early Mars: Journal of Geophysical Research, v. 113, E08005, 15 p., doi:10.1029/2007JE002962.

Jopling, A.V., 1966, Some procedures and techniques used in reconstructing the hydraulic parameters of a paleoflow regime: Journal of Sedimentary Petrology, v. 36, p. 5–49.

Kennedy, M., Droser, M., Mayer, L.M., Pevear, D., and Mrofka, D., 2006, Late Precambrian oxygenation: Inception of the clay mineral factory: Science, v. 311, p. 1446–1449, doi:10.1126/science.1118929.

Kerber, L., and Head, J.W.I., 2010, The age of the Medusae Fossae Formation: Evidence of Hesperian emplacement from crater morphology, stratigraphy, and ancient lava contacts: Icarus, v. 206, no. 2, p. 669–684, doi:10.1016/j.icarus.2009.10.001.

Kirkland, J.I., and Madsen, S.K., 2007, The Lower Cretaceous Cedar Mountain Formation, eastern Utah: The view up an always interesting learning curve, *in* Lund, W.R., ed., Field Guide to Geologic Excursions in Southern Utah: Geological Society of America Rocky Mountain Section 2007 Annual Meeting, St. George, Utah: Utah Geological Association Publication 35, 108 p.

Kirkland, J.I., Cifelli, R.L., Britt, B.B., Burge, D.L., DeCourten, F.L., Eaton, J.G., and Parrish, J.M., 1999, Distribution of vertebrate faunas in the

Cedar Mountain Formation, east-central Utah, *in* Gillette, D.D., ed., Vertebrate Paleontology in Utah: Utah Geological Survey Miscellaneous Publication 99-1, p. 201–217.

Kleinhans, M.G., 2005, Flow discharge and sediment transport models for estimating a minimum timescale of hydrological activity and channel and delta formation on Mars: Journal of Geophysical Research, v. 110, E12003, doi:10.1029/2005JE002521.

Knighton, D., 1998, Fluvial Forms and Processes: A New Perspective: New York, Oxford University Press, 338 p.

Komar, P.D., 1980, Modes of sediment transport in channelized water flows with ramifications to the erosion of the Martian outflow channels: Icarus, v. 42, p. 317–329, doi:10.1016/0019-1035(80)90097-4.

Landis, G.A., Blaney, D., Cabrol, N., Clark, B.C., Farmer, J., Grotzinger, J., Greeley, R., Richter, L., Yen, A., and MER Athena Science Team, 2004, Transient liquid water as a mechanism for induration of soil crusts on Mars [abs.]: Houston, Texas, Lunar and Planetary Institute, Lunar and Planetary Science Conference XXXV, abstract 2188 (CD-ROM).

Langbein, W.B., and Leopold, L.B., 1964, Quasi-equilibrium states in channel morphology: American Journal of Science, v. 262, p. 782–794, doi:10.2475/ajs.262.6.782.

Lawyer, G.F., 1972, Sedimentary features and paleoenvironment of the Dakota Sandstone (early Upper Cretaceous) near Hanksville, Utah: Brigham Young University Geology Studies, v. 19, p. 89–120.

LeDeit, L., Bourgeois, O., Mège, D., Hauber, E., Le Mouélic, S., Massé, M., Jaumann, R., Bibring, J.-P., 2010, Morphology, stratigraphy, and mineralogical composition of a layered formation covering the plateaus around Valles Marineris, Mars: Implications for its geological history: Icarus, v. 208, no. 2, p. 684–703, doi:10.1016/j.icarus.2010.03.012

Leopold, L.B., and Wolman, M.G., 1957, River channel patterns: Braided, meandering and straight: U.S. Geological Survey Professional Paper 282-B, p. 39–85.

Leopold, L.B., Wolman, M.G., and Miller, J.P., 1992, Fluvial Processes in Geomorphology: New York, Dover Publications, 535 p.

Lewis, K.W., and Aharonson, O., 2006, Stratigraphic analysis of the distributary fan in Eberswalde crater using stereo imagery: Journal of Geophysical Research, v. 111, E06001, 7 p., doi:10.1029/2005JE002558.

Lorenz, J.C., Cooper, S.P., and Olsson, W.A., 2006, Natural fracture distributions in sinuous, channel-fill sandstones of the Cedar Mountain Formation, Utah: The American Association of Petroleum Geologists Bulletin, v. 90, p. 1293–1308.

Lowe, D.R., 2007, A comment on "Weathering of quartz as an Archean climatic indicator" by N.H. Sleep and A.M. Hessler: Earth and Planetary Science Letters, v. 253, p. 530–533, doi:10.1016/j.epsl.2006.11.006.

Lucchitta, I., 1990, History of the Grand Canyon and of the Colorado River in Arizona, *in* Beus, S.S., and Morales, M., eds., The Grand Canyon Geology: New York, Oxford University Press, p. 311–332.

Maizels, J.K., 1983, Palaeovelocity and palaeodischarge determination for coarse gravel deposits, *in* Gregory, K.J., ed., Background to Paleohydrology: A Perspective: New York, John Wiley and Sons, p. 101–139.

Maizels, J.K., 1987, Plio-Pleistocene raised channel systems of the western Sharqiya (Wahiba), Oman, *in* Frostick, L., and Reid, L., eds., Desert Sediments: Ancient and Modern: Geological Society [London] Special Publication 35, p. 31–50.

Malin, M.C., and Edgett, K.S., 2000, Evidence for recent groundwater seepage and surface runoff on Mars: Science, v. 288, p. 2330–2335, doi:10.1126/science.288.5475.2330.

Malin, M.C., and Edgett, K.S., 2001, Mars Global Surveyor Mars Orbiter Camera: Interplanetary cruise through primary mission: Journal of Geophysical Research, v. 106, no. E10, p. 23,429–23,570.

Malin, M.C., and Edgett, K.S., 2003, Evidence for persistent flow and aqueous sedimentation on early Mars: Science, v. 302, p. 1931–1934, doi:10.1126/science.1090544.

Malin, M.C., Edgett, K.S., Posiolova, L.V., McColley, S.M., and Noe Dobrea, E.Z., 2006, Present-day impact cratering rate and contemporary gully activity on Mars: Science, v. 314, p. 1573–1577, doi:10.1126/science.1135156.

Mandt, K.E., de Silva, S., Zimbelman, J.R., and Crown, D.A., 2008, Origin of the Medusae Fossae Formation, Mars: Insights from a synoptic approach: Journal of Geophysical Research, v. 113, 15 p., doi:10.1029/2008JE003076.

Mangold, N., Quantin, C., Ansan, V., Delacourt, C., and Allemand, P., 2004, Evidence for precipitation on Mars from dendritic valleys in the Valles Marineris area: Science, v. 305, p. 78–81, doi:10.1126/science.1097549.

Mangold, N., Ansan, V., Masson, P., Quantin, C., and Neukum, G., 2008, Geomorphic study of fluvial landforms on the northern Valles Marineris plateau, Mars: Journal of Geophysical Research, v. 113, E08009, doi:10.1029/2007JE002985.

Mars Channel Working Group, 1983, Channels and valleys on Mars: Geological Society of America Bulletin, v. 94, no. 9, p. 1035–1054, doi:10.1130/0016-7606(1983)94<1035:CAVOM>2.0.CO;2.

Meek, F.G., and Hayden, F.V., 1862, Description of new Lower Silurian (Primoridal), Jurassic, Cretaceous and Tertiary fossils, collected in Nebraska, by the exploring expedition under the command of Capt. Wm. F. Reynolds, U.S. Top. Engineers, with some remarks on the rocks from which they were obtained: Academy of Natural Sciences of Philadelphia Proceedings, v. 13, p. 415–447.

Moore, J.M., and Howard, A.D., 2005, Large alluvial fans on Mars: Journal of Geophysical Research, v. 110, 24 p., doi:10.1029/2004JE002352.

Moore, J.M., Howard, A.D., Dietrich, W.E., and Schnek, P.M., 2003, Martian layered fluvial deposits: Implications for Noachian climate scenarios: Geophysical Research Letters, v. 30, 2292, doi:10.1029/2003GL019002.

Morris, R.V., Ruff, S.W., Gellert, R., Ming, D.W., Arvidson, R.E., Clark, B.C., Golden, D.C., Siebach, K., Klingelhöfer, G., Schröder, C., Fleischer, I., Yen, A., and Squyres, S.W., 2010, Identification of carbonate-rich outcrops on Mars by the *Spirit* rover: Science, v. 329, p. 421–424, doi:10.1126/science.1189667.

Mustard, J.F., Murchie, S.L., Pelkey, S.M., et al., 2008, Hydrated silicate minerals on Mars observed by the *Mars Reconnaissance Orbiter* CRISM instrument: Nature, v. 454, p. 305–309, doi:10.1038/nature07097.

Mullens, T.E., and Freeman, V.L., 1957, Lithofacies of the Salt Wash Member of the Morrison Formation, Colorado Plateau: Geological Society of America Bulletin, v. 68, p. 505–526, doi:10.1130/0016-7606(1957)68[505:LOTSWM]2.0.CO;2.

National Imagery and Mapping Agency, 2000, Department of Defense World Geodetic System 1984, Its Definition and Relationships with Local Geodetic Systems: NIMA Technical Report TR8350.2, Third Edition, 3 January 2000: http://earth-info.nga.mil/GandG/publications/tr8350.2/wgs-84fin.pdf (last accessed 8 July 2011).

Newsom, H.E., Hagerty, J.J., and Thorsos, I.E., 2001, Location and sampling of aqueous and hydrothermal deposits in Martian impact craters: Astrobiology, v. 1, no. 1, p. 71–88.

Newsom, H.E., Lanza, N.L., Ollila, A.M., Wiseman, S.M., Roush, T.L., Marzo, G.A., Tornabene, L.L., Okubo, C.H., Osterloo, M.M., Hamilton, V.E., and Crumpler, L.S., 2010, Inverted channel deposits on the floor of Miyamoto crater, Mars: Icarus, v. 205, p. 64–72, doi:10.1016/j.icarus.2009.03.030.

Nuccio, V.F., and Condon, S.M., 1996, Burial and thermal history of the Paradox basin, Utah and Colorado, and petroleum potential of the Middle Pennsylvanian Paradox Formation: U.S. Geological Survey Bulletin 2000-O, p. 41.

Nuccio, V.F., and Roberts, L.N.R., 2003, Chapter 4—Thermal maturity and oil and gas generation history of petroleum systems in the Uinta–Piceance province, Utah and Colorado, *in* Petroleum Systems and Geologic Assessment of Oil and Gas in the Uinta–Piceance Province, Utah and Colorado: U.S. Geological Survey Digital Data Series DDS-69-B, p. 35, http://pubs.usgs.gov/dds/dds-069/dds-069-b/REPORTS/Chapter_4.pdf (last accessed 14 July 2011).

Osterloo, M.M., Hamilton, V.E., Bandfield, J.L., Glotch, T.D., Baldridge, A.M., Christensen, P.R., Tornabene, L.L., and Anderson, F.S., 2008, Chloride-bearing materials in the Southern Highlands of Mars: Science, v. 319, p. 1651–1654, doi:10.1126/science.1150690.

Pain, C.F., Clarke, J.D.A., and Thomas, M., 2007, Inversion of relief on Mars: Icarus, v. 190, p. 478–491, doi:10.1016/j.icarus.2007.03.017.

Parker, G., 1976, On the cause and characteristic scales of meandering and braiding in rivers: Journal of Fluid Mechanics v. 76, p. 457–480.

Pelkey, S.M., Mustard, J.F., Murchie, S., Clancy, R.T., Wolff, M., Smith, M., Milliken, R., Bibring, J.P., Gendrin, A., Poulet, F., Langevin, Y., and Gondet, B., 2007, CRISM multispectral summary products: Parameterizing mineral diversity on Mars from reflectance: Journal of Geophysical Research, v. 112, E08S14, doi:10.1029/2006JE002831.

Peterson, F., 1988, Stratigraphy and nomenclature of Middle and Upper Jurassic rocks, western Colorado Plateau, Utah and Arizona, *in* Revisions to Stratigraphic Nomenclature of Jurassic and Cretaceous Rocks of the Colorado Plateau: U.S. Geological Survey Bulletin 1633-B, p. B13–56.

Peterson, J.A., 1972, Jurassic System, *in* Mallory, W.W., ed., Geologic Atlas of the Rocky Mountains: Denver, Colorado, Rocky Mountain Association of Geologists, p. 177–189.

Prothero, D.R., Dott, R.H., and Dott, R.H.J., 2003, Evolution of the Earth: New York, McGraw-Hill Science, 576 p.

Rathbun, J.A., and Squyres, S.W., 2002, Hydrothermal systems associated with Martian impact craters: Icarus, v. 157, no. 2, p. 362–372, doi:10.1006/icar.2002.6838.

Rhodes, D.D., 1980, Exhumed topography—A case study of the Stanislaus Table Mountain, California, *in* Reports of Planetary Geology Program—1980: NASA Technical Memorandum 82385 p. 397–399.

Rice, M.S., 2010, Testable Hypotheses and Candidate Science Targets Within the Eberswalde Landing Ellipse, Mars Science Laboratory Landing Site Workshop [abs.]: Pasadena, California.

Rigby, J.K., 1976, Northern Colorado Plateau, K/H Geology Field Guide Series: Dubuque, Iowa, Kendall/Hunt Publishing Company, 207 p.

Rogers, A.D., and Christensen, P.R., 2007, Surface mineralogy of Martian low-albedo regions from MGS-TES data: Implications for upper crustal evolution and surface alteration: Journal of Geophysical Research, v. 112, E01003, 18 p., doi:10.1029/2006JE002727.

Ruddiman, W.F., Prell, W.L., and Raymo, M.E., 1989, Late Cenozoic uplift in southern Asia and the American West: Rationale for general circulation modeling experiments: Journal of Geophysical Research, v. 94, no. D15, p. 18,379–18,391, doi:10.1029/JD094iD15p18379.

Sahagian, D., Proussevitch, A., and Carlson, W., 2002, Timing of Colorado Plateau uplift: Initial constraints from vesicular basalt-derived paleoelevations: Geology, v. 30, no. 9, p. 807–810, doi:10.1130/0091-7613(2002)030<0807:TOCPUI>2.0.CO;2.

Segura, T.L., Toon, O.B., Colaprete, A., and Zahnle, K., 2002, Environmental effects of large impacts on Mars: Science, v. 298, no. 5600, p. 1977–1980.

Segura, T.L., Toon, O.B., Colaprete, A., and Zahnle, K., 2008, A sustained greenhouse climate and erosion period on Mars following an impact event [abs.]: Houston, Texas, Lunar and Planetary Institute, Lunar and Planetary Science Conference XXXIX, abstract 1793 (CD-ROM).

Seminara, G., 2006, Meanders: Journal of Fluid Mechanics, v. 554, p. 271–297, doi:10.1017/S0022112006008925.

Shipton, Z.K., Evans, J.P., Kirschner, D., Kolesar, P.T., Williams, A.P., and Heath, J., 2004, Analysis of CO_2 leakage through "low-permeability" faults from natural reservoirs in the Colorado Plateau, east-central Utah, *in* Baines, S.J., and Worden, R.H., eds., Geological Storage of Carbon Dioxide: Geological Society of London Special Publication 233, p. 43–58.

Stokes, W.L., 1944, Morrison Formation and related deposits in and adjacent to the Colorado Plateau: Geological Society of America Bulletin, v. 552, p. 951–992.

Stokes, W.L., 1952, Lower Cretaceous in the Colorado Plateau: The American Association of Petroleum Geologists Bulletin, v. 36, p. 1766–1776.

Stokes, W.L., 1961, Fluvial and aeolian sandstone bodies in the Colorado Plateau, *in* Petersen, J.A., and Osmond, J.C., eds., Geometry of Sandstone Bodies: American Association of Petroleum Geologists Bulletin, p. 151–178.

Tanaka, K.L., 1986, The stratigraphy of Mars: Journal of Geophysical Research, v. 91, no. B13, p. E139–E158, doi:10.1029/JB091iB13p0E139.

Tanaka, K.L., and Kolb, E.J., 2001, Geologic history of the polar regions of Mars based on *Mars Global Surveyor* data: I. Noachian and Hesperian Periods: Icarus, v. 154, p. 3–21, doi:10.1006/icar.2001.6675.

Trimble, L.M., and Doelling, H.H., 1978, Geology and uranium-vanadium deposits of the San Rafael River mining area, Emery County, Utah: Utah Geological and Mineralogical Survey Bulletin, v. 113, p. 156–194.

Turner, C.E., and Fishman, N.S., 1991, Jurasic Lake T'oo'dichi': A large alkaline, saline lake, Morrison Formation, eastern Colorado Plateau: Geological Society of America Bulletin, v. 103, p. 538–558, doi:10.1130/0016-7606(1991)103<0538:JLTODA>2.3.CO;2.

Turner, C.E., and Peterson, F., 2004, Reconstruction of the Upper Jurassic Morrison Formation extinct ecosystem—A synthesis: Journal of Sedimentary Geology, v. 167, p. 309–355, doi:10.1016/j.sedgeo.2004.01.009.

van den Berg, J.H., 1995, Prediction of alluvial channel pattern of perennial rivers: Geomorphology, v. 12, p. 259–279, doi:10.1016/0169-555X(95)00014-V.

Visher, G.S., 1965, Use of vertical profile in environmental reconstruction: American Association of Petroleum Geologists Bulletin, v. 49, p. 41–61.

Weitz, C.M., Milliken, R.E., Grant, J.A., McEwen, A.S., Williams, R.M.E., Bishop, J.L., and Thomson, B.J., 2010, *Mars Reconnaissance Orbiter* observations of light-toned layered deposits and associated fluvial landforms on the plains adjacent to Valles Marineris: Icarus, v. 205, no. 1, p. 73–102, doi:10.1016/j.icarus.2009.04.017.

Wentworth, S.J., Gibson, E.K., Velbel, M.A., and McKay, D.S., 2005, Antarctic Dry Valleys and indigenous weathering in Mars meteorites: Implications for water and life on Mars: Icarus, v. 174, no. 2, p. 383–395.

Williams, P.F., and Hackman, R.J., 1971, Geology of the Salina Quadrangle, Utah: U.S. Geological Survey Miscellaneous Investigations Map I-1591-A, scale 1:250,000, 1 sheet, reprinted 1983.

Williams, R.M.E., 2007, Global spatial distribution of raised curvilinear features on Mars [abs.]: Houston, Texas, Lunar and Planetary Institute, Lunar and Planetary Science Conference XXXVIII, abstract 1821 (CD-ROM).

Williams, R.M.E., and Phillips, R.J., 2001, Morphometric measurements of Martian valley networks from Mars Orbiter Laser Altimeter (MOLA) data: Journal of Geophysical Research, v. 106, no. E10, p. 23,737–23,751, doi:10.1029/2000JE001409.

Williams, R.M.E., Malin, M.C., and Edgett, K.S., 2005, Remnants of the courses of fine-scale, precipitation-fed runoff streams preserved in the Martian rock record [abs.]: Houston, Texas, Lunar and Planetary Institute, Lunar and Planetary Science Conference XXXVI, abstract 1099 (CD-ROM).

Williams, R.M.E., Chidsey, T.C., Jr., and Eby, D.E., 2007, Exhumed paleochannels in central Utah—Analogs for raised curvilinear features on Mars, *in* Willis, G.C., Hylland, M.D., Clark, D.L., and Chidsey, T.C., Jr., eds., Central Utah—Diverse Geology of a Dynamic Landscape: Utah Geological Association Publication 36, p. 220–235.

Williams, R.M.E., Eby, D.E., and Chidsey, T.C., Jr., 2009a, Early cementation is a key phase to preservation of "inverted paleochannels" on Mars and Earth: Implications for diagenetic water on Mars [abs.], *in* Pascucci, V., and Andreucci, S., eds., 27th IAS Meeting of Sedimentologists: Sassari, Sardinia, Italy International Association of Sedimentologists, p. 717.

Williams, R.M.E., Irwin, R.P., III, and Zimbelman, J.R., 2009b, Evaluation of paleohydrologic models for terrestrial inverted channels: Implications for application to Martian sinuous ridges: Geomorphology, v. 107, p. 300–315, doi:10.1016/j.geomorph.2008.12.015.

Wilson, L., Ghatan, G.J., Head, J.W.I., and Mitchell, K.L., 2004, Outflow channels: A reappraisal of the estimation of water flow velocities from water depths, regional slopes, and channel floor properties: Journal of Geophysical Research, v. 109, E09003, 10 p., doi:10.1029/2004JE002281.

Wood, L.J., 2006, Quantitative geomorphology of the Mars Eberswalde delta: Geological Society of America Bulletin, v. 118, p. 557–566, doi:10.1130/B25822.1.

Young, G.R., 1960, Dakota Group of Colorado Plateau: The American Association of Petroleum Geologists Bulletin, v. 44, p. 156–194.

Manuscript Accepted by the Society 2 February 2011

Printed in the USA

Field guide to exhumed paleochannels near Green River, Utah:
Terrestrial analogs for sinuous ridges on Mars

Rebecca M. E. Williams[1], Rossman P. Irwin III[1], James R. Zimbelman[2], Thomas C. Chidsey, Jr.[3], David E. Eby[4]

[1]Planetary Science Institute, 1700 East Fort Lowell Rd., Suite 106, Tucson, AZ 85179
[2]Center for Earth and Planetary Studies, National Air and Space Museum,
Smithsonian Institution, Independence Ave. at Sixth St. SW,
MRC 315, Washington, DC 20013-7012
[3]Utah Geological Survey, P. O. Box 146100, Salt Lake City, UT 84114-6100
[4]Eby Petrography and Consulting, 2830 W. 9th Ave. Denver, CO 80204.

SUPPLEMENTAL MATERIALS

SUPPLEMENTAL FIGURES

For all photomicrographs, the following key is used:
PL = Plain Light; XN = Crossed Nicols; AP = Gypsum Accessory Plate; ND = Neutral Density filter.

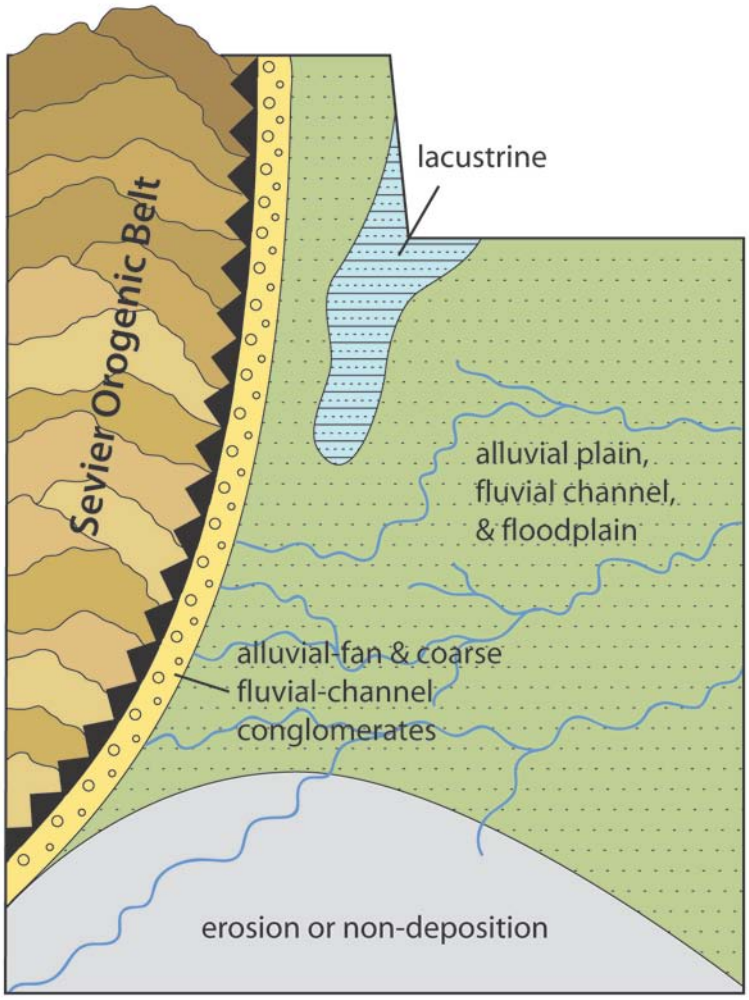

Supplemental Figure 1. Paleogeographic map of Utah during Ruby Ranch time (Aptian to middle Albian) with Sevier orogenic belt in western Utah and various fluvial depositional environments present in east-central Utah (Figure from Williams et al., 2007b, modified from Elder and Kirkland, 1993; Kirkland et al., 1998).

Supplemental Figure 2. View to the east of Derr's (1974) inverted channel 2 in the Brushy Basin Member of the Morrison Formation and location of stop 1. See Figure 8 for vantage point 'P' where picture was taken. Ridge along the skyline is the Ferroan Sandstone Member in the lower part of the Mancos Shale. Note truck for scale. Photo by T. Chidsey.

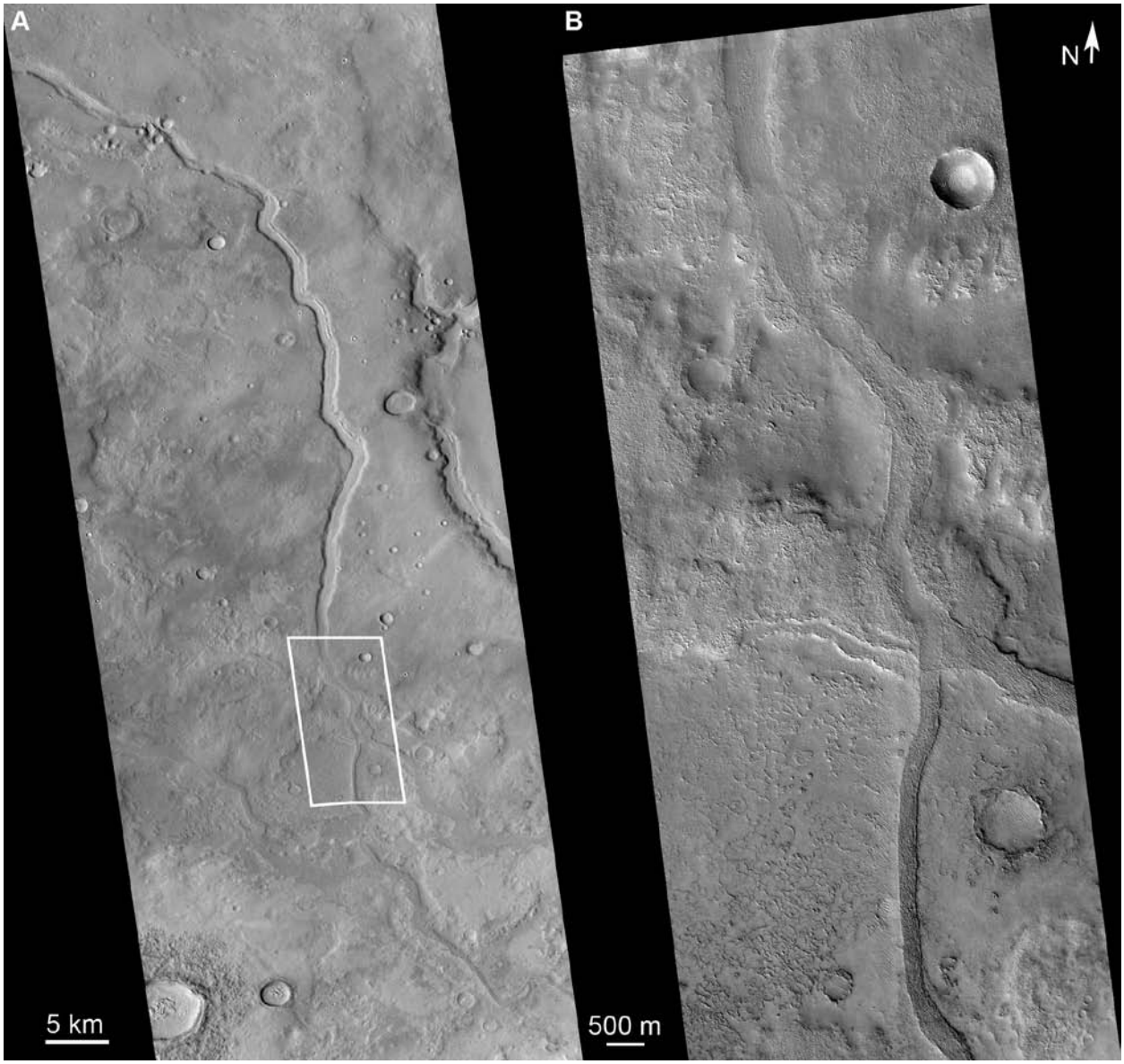

Supplemental Figure 3. A) Negative relief valley network (top of image) transitions to a low relief plateau (sinuous ridge at bottom) near 32° N, 314° W in Arabia Terra. White box marks location of panel B. Illuminati on from the lower left in this subscene of CTX image P15_006990_2127. B) Subscene of HiRISE image PSP_005355_2125 showing transition zone. Illumination is from the left (note impact crater at upper right in panel B). Image modified from original NASA/JPL/University of Arizona.

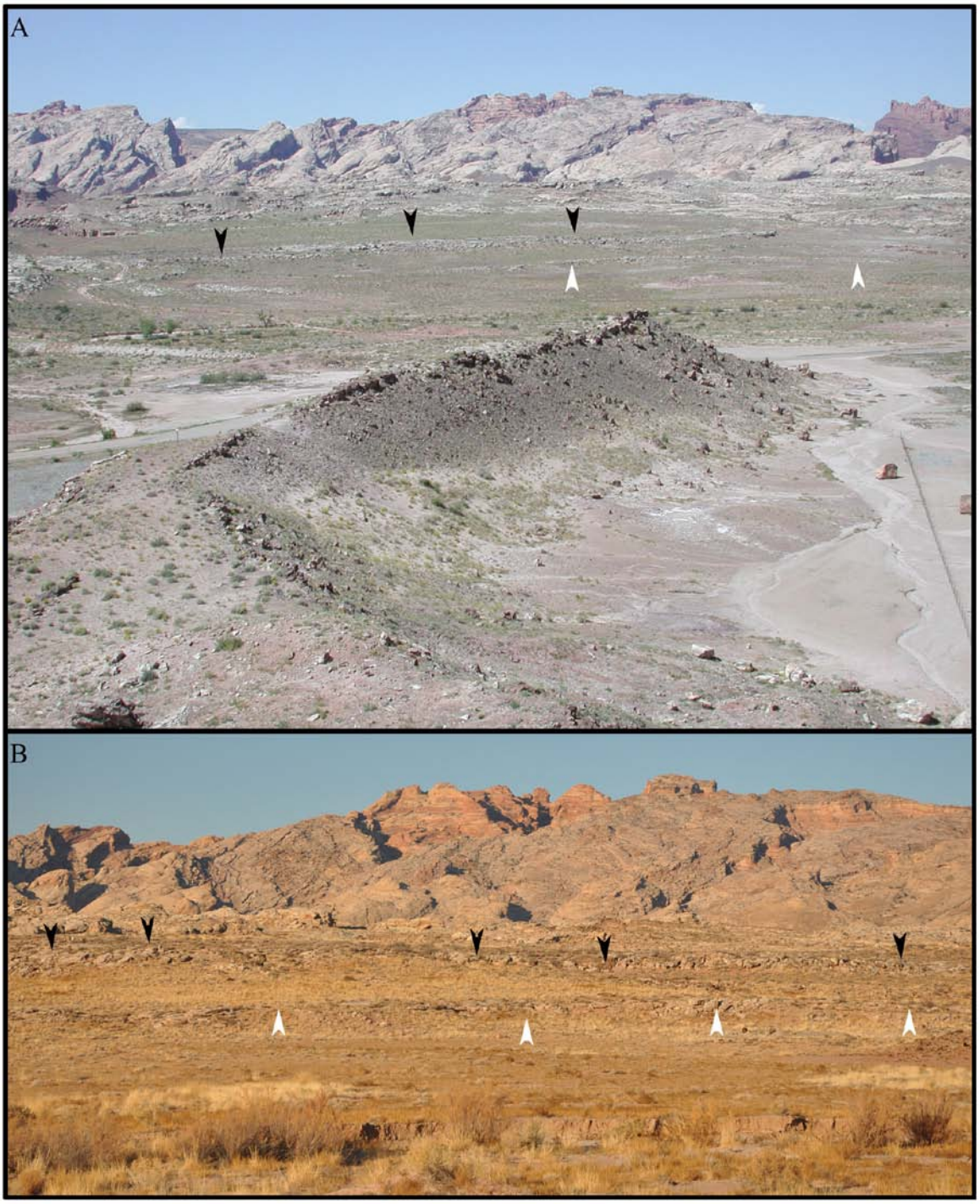

Supplemental Figure 4. A) View to the west from a nearby hill where two low-relief (<2 m) inverted channels are marked by black and white arrows. See Figure 8 for vantage point 'P' where the picture was taken. The San Rafael Swell is in the background. Width of scene at the location of the black arrows is ~0.5 km. Photo by T. Chidsey. B**)** Ground-based photo of same site shows that the surface expression of these inverted channels (marked by white and black arrows) is very subtle. Photo by R. Williams.

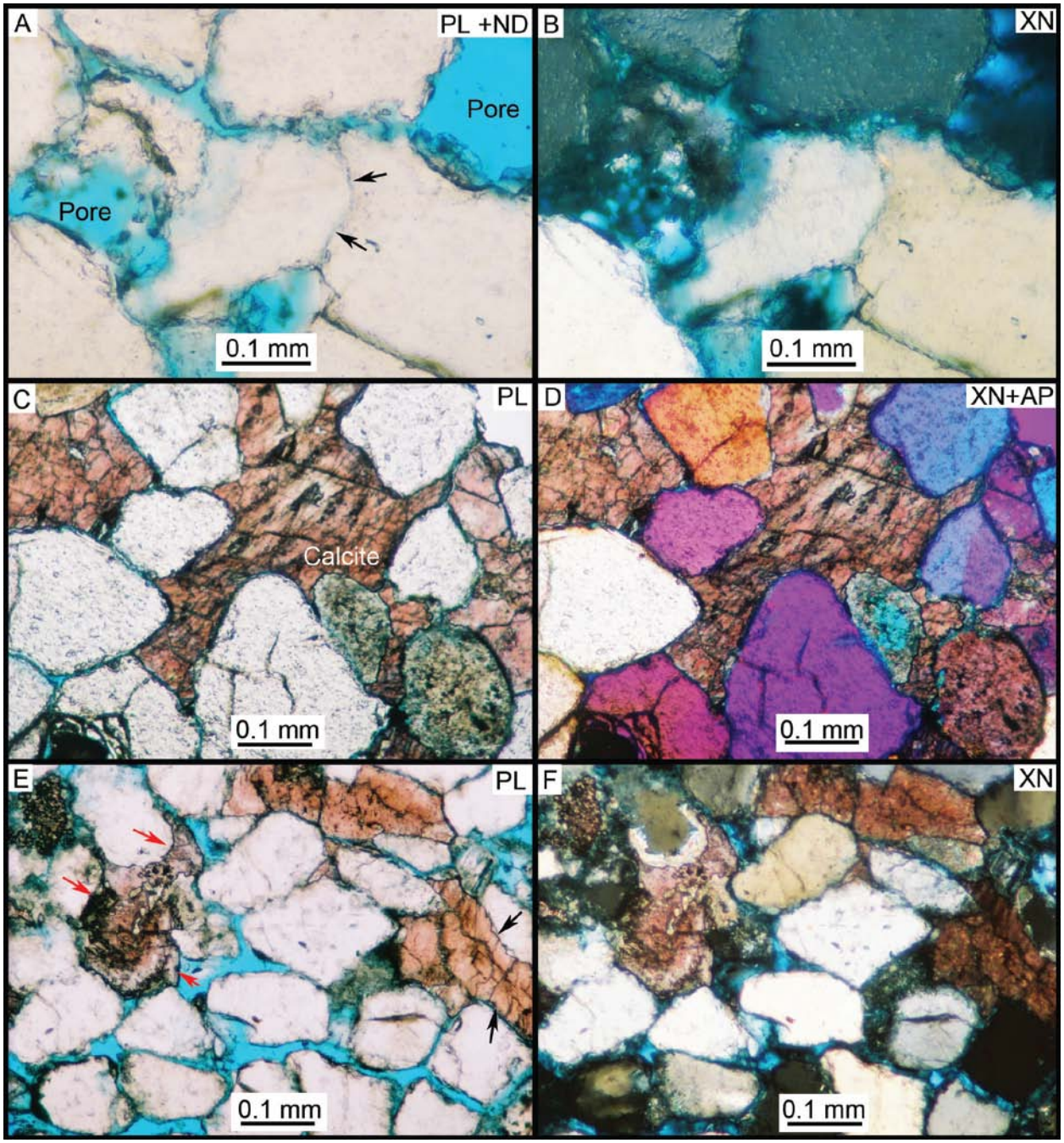

Supplemental Figure 5. Photomicrographs from samples of cemented channel materials in the Brushy Basin Member of the Morrison Formation (Figure 8, stop 2). Examples A-D are from site L and examples E-F are from site M. A) Low-resolution view of quartz sandstone with extensive calcite cement. 50X B) Interpenetrating quartz grain contacts (black arrows) provide evidence of burial. 250X C) Sparry calcite cement is pink due to Alizarin Red-S staining. 200X D) Same view with XN+AP. 200X E) Adjacent pores have different composition: calcite (black arrows) and ferroan calcite (red arrows). Dissolution pores (blue voids) are also present. 200X F) Same view with XN. Note pressure-solution grain contacts. 200X

Supplemental Figure 6. Several examples of outcrop exposures at the base of paleochannels in the Ruby Ranch Member. A) In channel D, muddy deposits are protected by overlying channel deposits, forming an overhang in the picture. Green and yellow-brown mudstone subjacent to the channel base formed in a reducing environment at the channel-floodplain interface. Photo by R. Williams. B) In places, there are large (~50 cm diameter) limestone rip-up clasts, likely lacustrine deposits that were reworked during high flow events. This example is from channel A. Photo by J. Zimbelman. C) Elsewhere the base of channel D is marked by a basal conglomerate with pedogenic carbonate nodules up to 10 cm in diameter; a similar basal conglomerate is observed elsewhere in the Cedar Mountain Formation to the north (Currie, 1998). Photo by R. Williams.

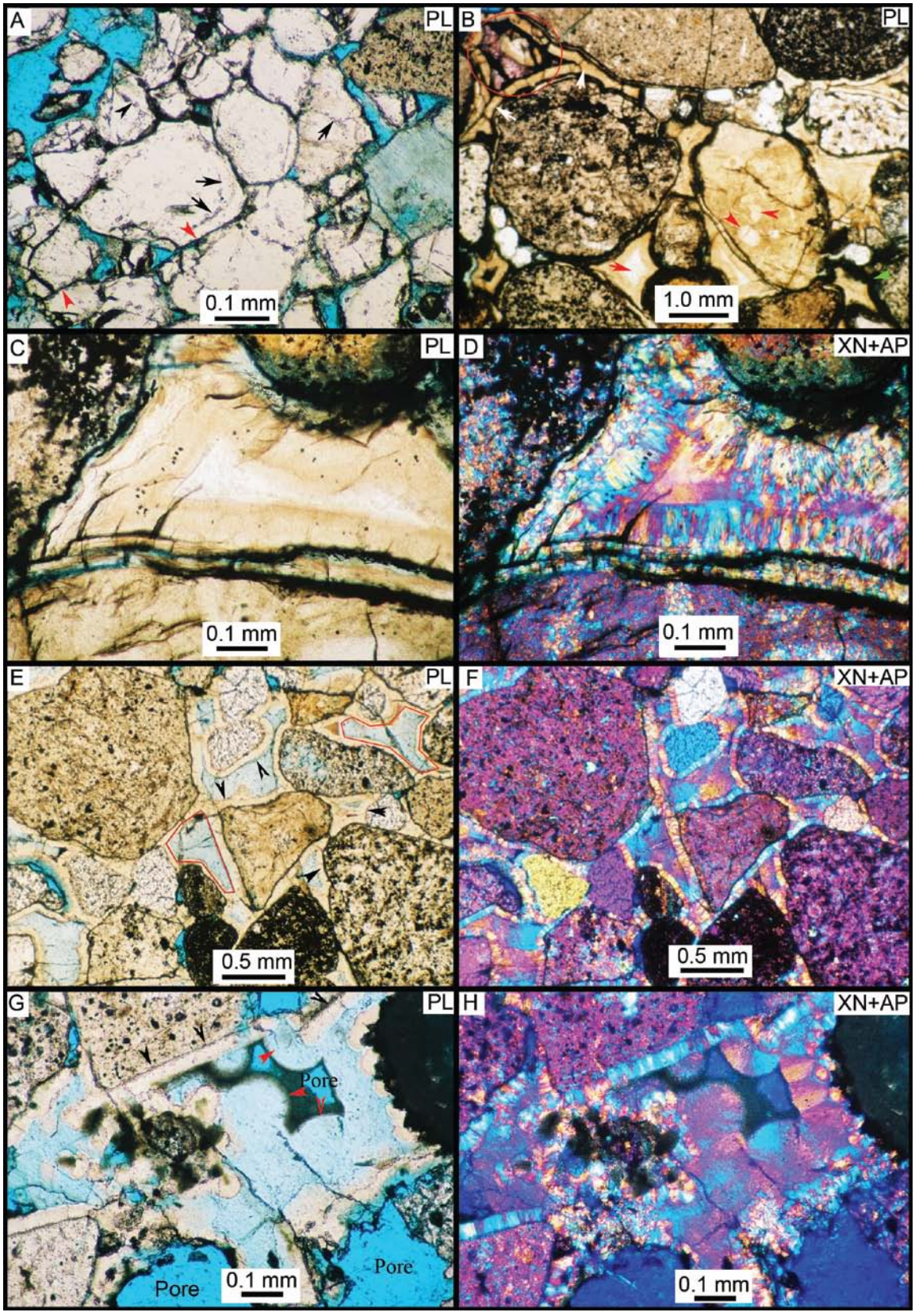

Supplemental Figure 7.

Supplemental Figure 7. Photomicrographs from samples of cemented channel materials in the Cedar Mountain Formation. Sample locations are marked on Figure 10B with example A from site E, examples B-D from site F and examples E-H from site G. A) Quartz-cemented coarse sandstone with secondary porosity (blue voids). Dust lines (arrows) demarcate quartz grain and silica overgrowth cement boundary. Linear grain contacts (red arrows) are evidence for pressure solution modification and indicate the specimen was largely uncemented prior to burial. Plain light (PL) 160X. B) Sandstone with multiple stages of silica cement formed under near-surface conditions: isopachous silica cements encircling grains (white arrows) form in phreatic pores, pore-filling silica cement is dense and brownish (green arrow), and third-generation crystalline cement with white core (red arrows). Alizarin Red-S staining highlights minor, late-stage calcite cement (red circle). PL 18.5X. C) Pore-filling siliceous cement. PL 160X. D) Same view as previous with crossed Nichols (XN) and gypsum accessory plate (AP) which highlights the fibrous character of the chalcedony cement. 160X. E) Isopachous silica cement (black arrows) encircles grains. Light blue color (from blue impregnated epoxy; red outline) indicates the microporous nature of the pore-filling silica cement. 40X. F) Same view as previous with XN+AP. Fibrous character of chalcedony cement is evident. 40X. G) Isopachous silicious cement (black arrows) and secondary botryoidal , microporous silicious cements (red arrows) in pore centers. 130X. H) Same view as previous with XN+AP shows the radiating fiber of the botryoidal cement. 130X.

Supplemental Figure 8. Oblique aerial photograph to the southeast of a sinuous section of channel A in the Cedar Mountain Formation. Water gap marked by black arrow at top right. Older channels (white arrow at center bottom) beneath the main trunk channel are preserved only on the north side. Image width in foreground is ~1.8 km. Illumination is from the upper left. Photo by R. Williams.

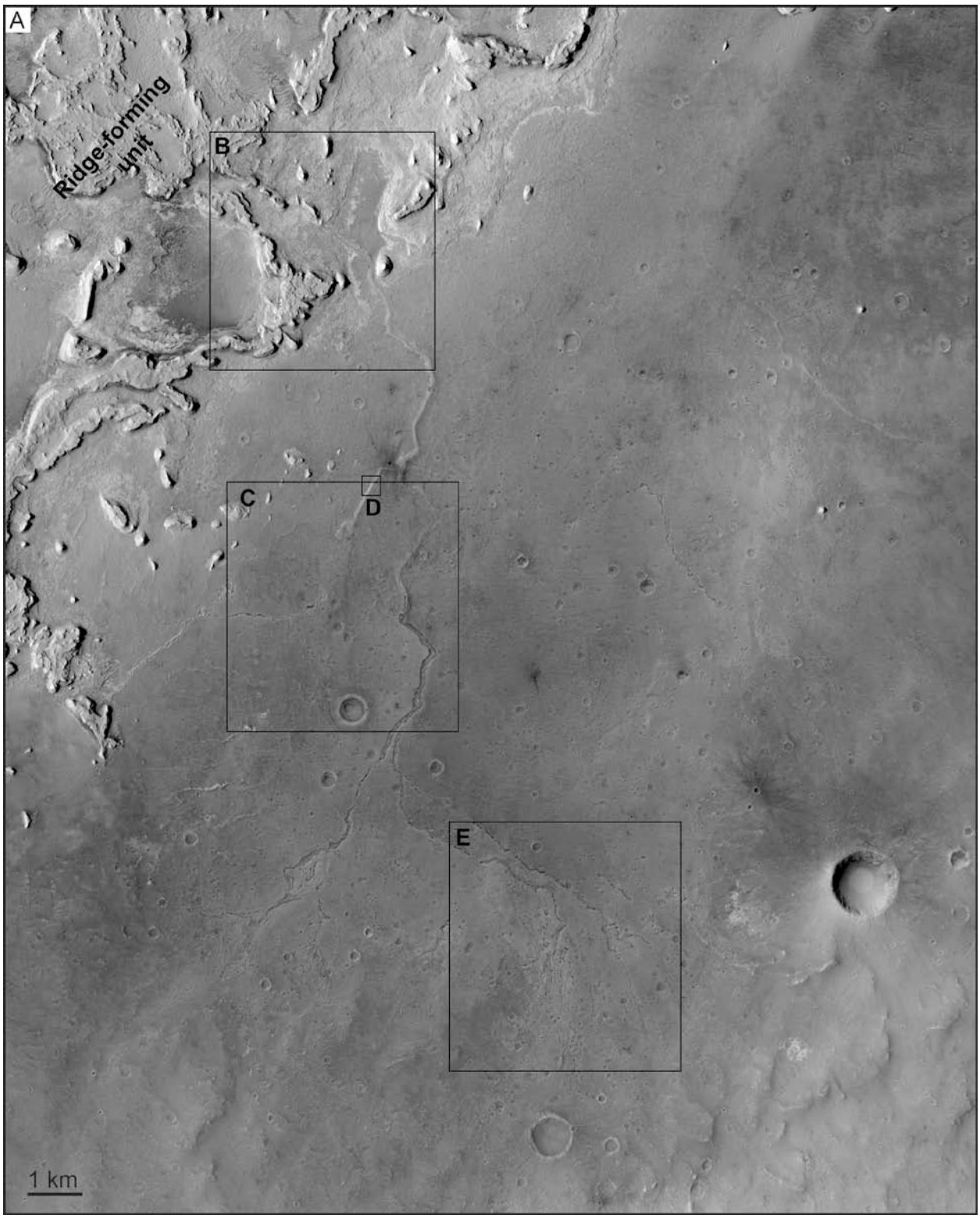

Supplemental Figure 9A.

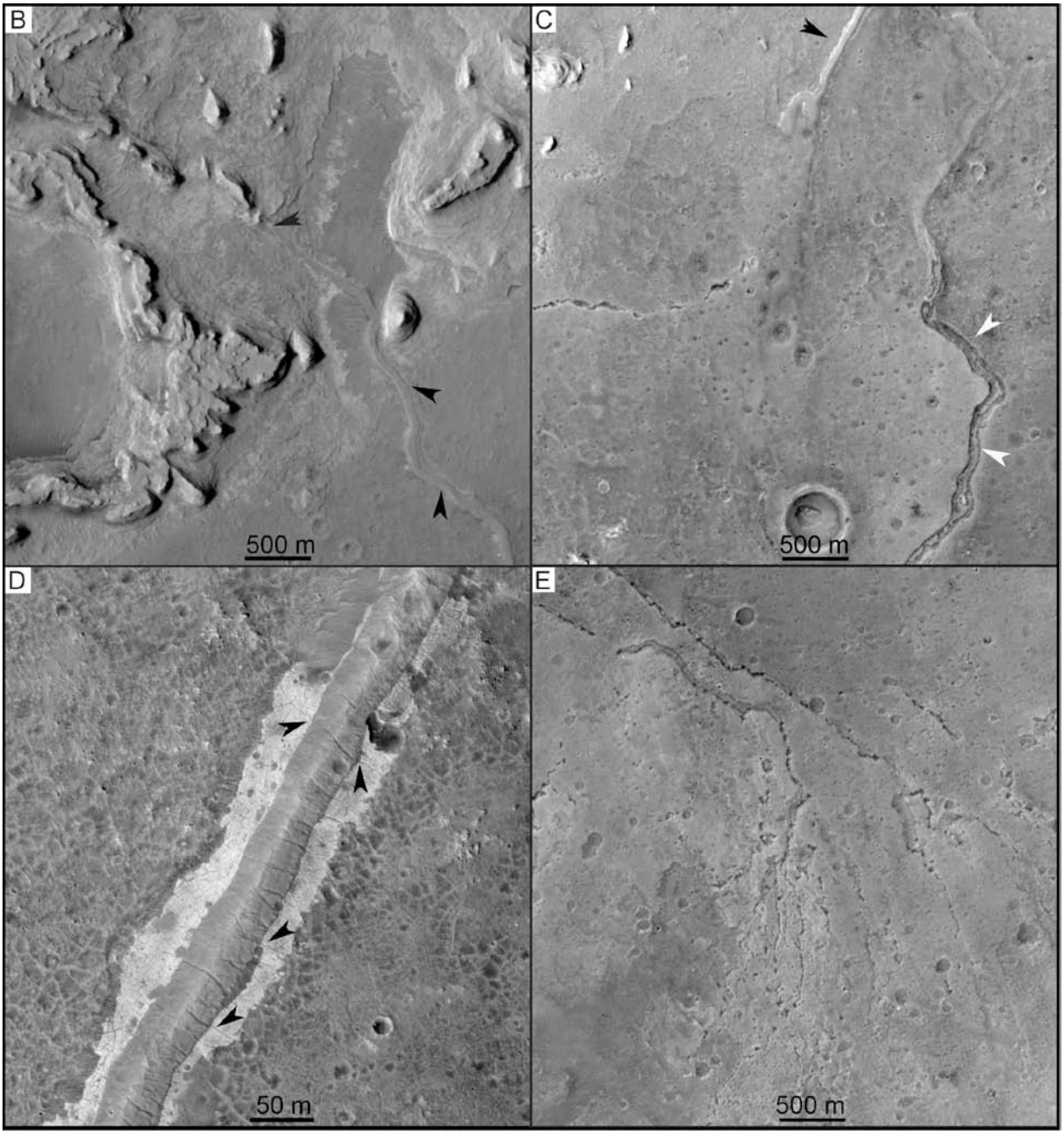

Supplemental Figure 9. A) Branching landform in Meridiani Planum that exhibits variations in preservation style from positive to negative relief. Black boxes in A are Enlargement of subscenes from panel A are presented in panels B-E. Northern portion of system (B), presumably the downstream section, is buried beneath rock layers (black arrow). The landform transitions from positive relief (low-relief ridge marked by black arrow) to negative relief trough (white arrows in C) that has a medial ridge in places. The southern portion of the landform is marked by a series of aligned pits that trace out the branching pattern (E). At higher resolution (D), the stratigraphic relationship is evident with the low-relief, light-toned ridge (the inverted channel) capped by a narrow band of the former overburden. The cracked pattern on the light-toned ridge and superposing material (cracks are sometimes traverse across the two materials, marked by black arrows) differ in size and configuration from the polygonal pattern on the surrounding plains. Panels A-C and E are subframes of CTX image P03_002390_1840 near 4.6˚ N, 1.3˚ W. Panel D is subframe of HiRISE PSP_004091_1845. Illumination is from left for all images.

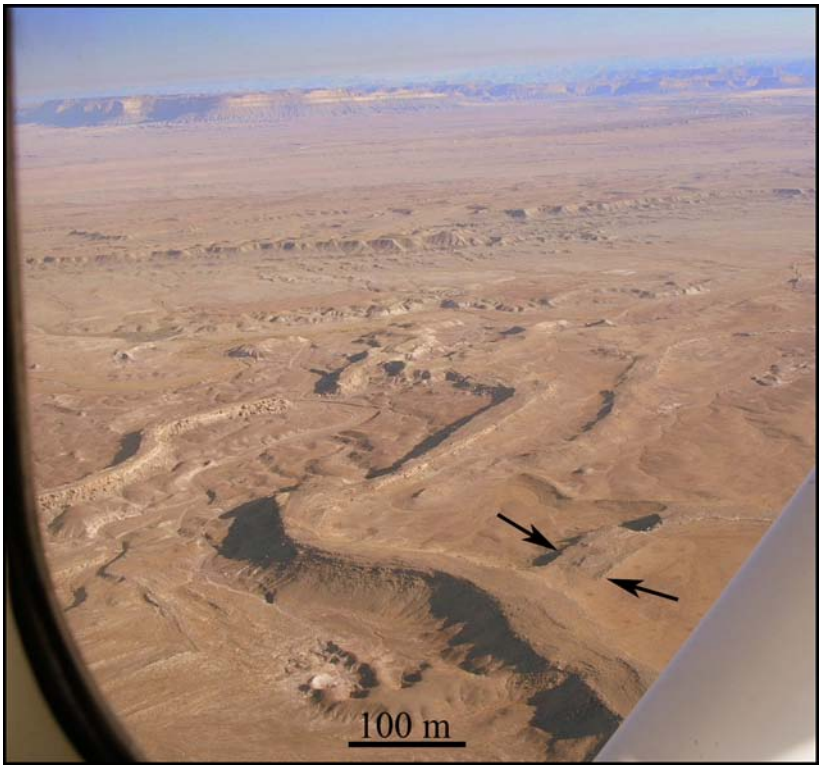

Supplemental Figure 10. Oblique aerial photograph of two channel segments in the Cedar Mountain Formation looking northward, at the location near the labels F and G in Figure 10. The apparent bifurcation marked by black arrows is actually two segments at two different topographic and stratigraphic levels. The inverted paleochannel segment from top to bottom (north to south, segment D) in image is stratigraphically higher than the paleochannel segment that extends to the right (westernmost section of segment B). Scale bar is for image foreground. The Late Cretaceous Book Cliffs (e.g. Young, 1955), which form the northern rim of the Colorado Plateau in eastern Utah, are visible in the background. Photo by R. Williams.

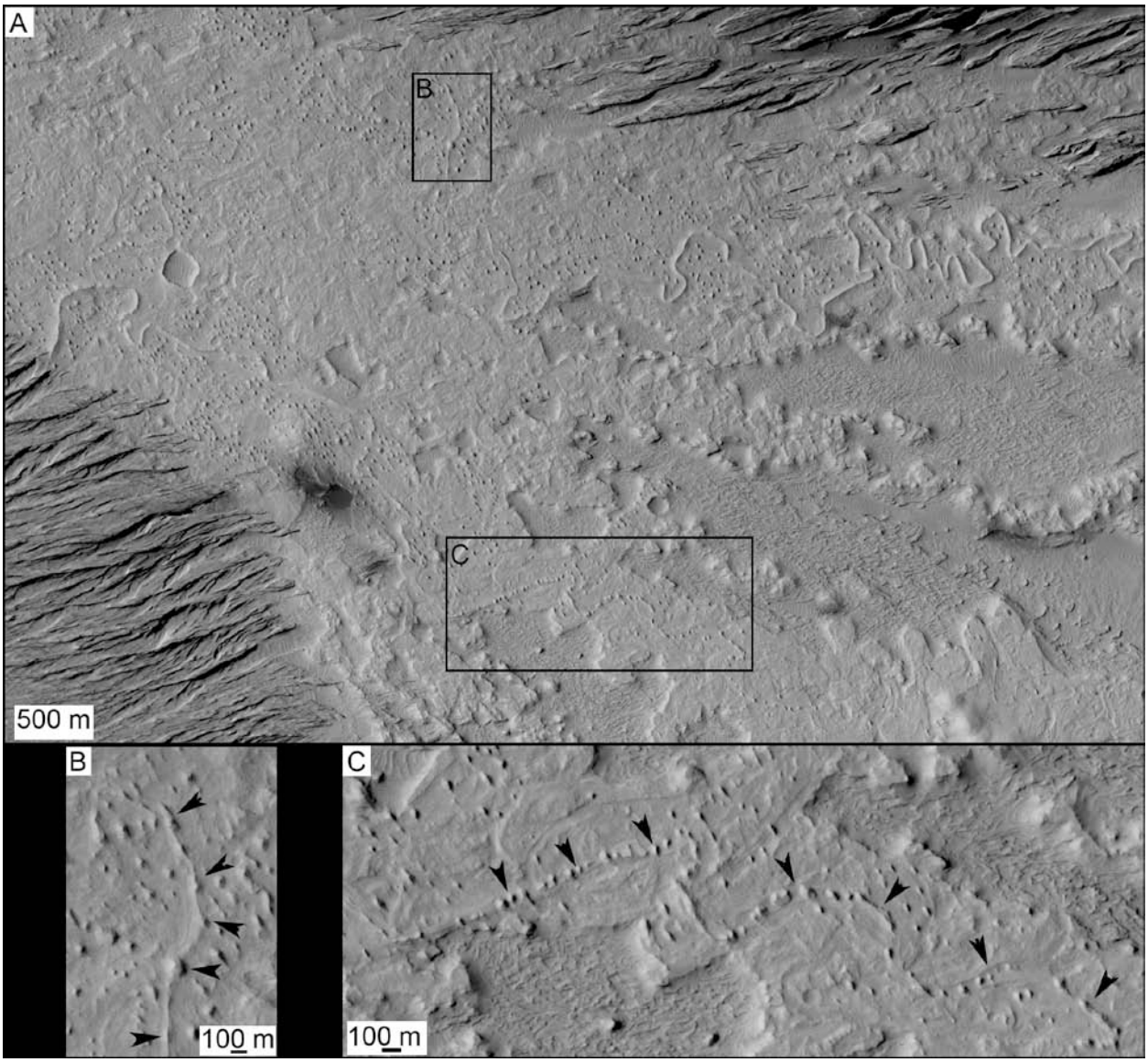

Supplemental Figure 11. A) Sinuous ridges in the Aeolis/Zephyria Plana region immediately east of the location in Figure 6. Black boxes are approximate regions enlarged in panels B and C, which show areas where eolian erosion has modified former sinuous ridges into aligned knobs and mesas (black arrows). Subframe of CTX image P03_002081_1751 is located near 5˚ S, 205˚ W. Illumination is from lower left.

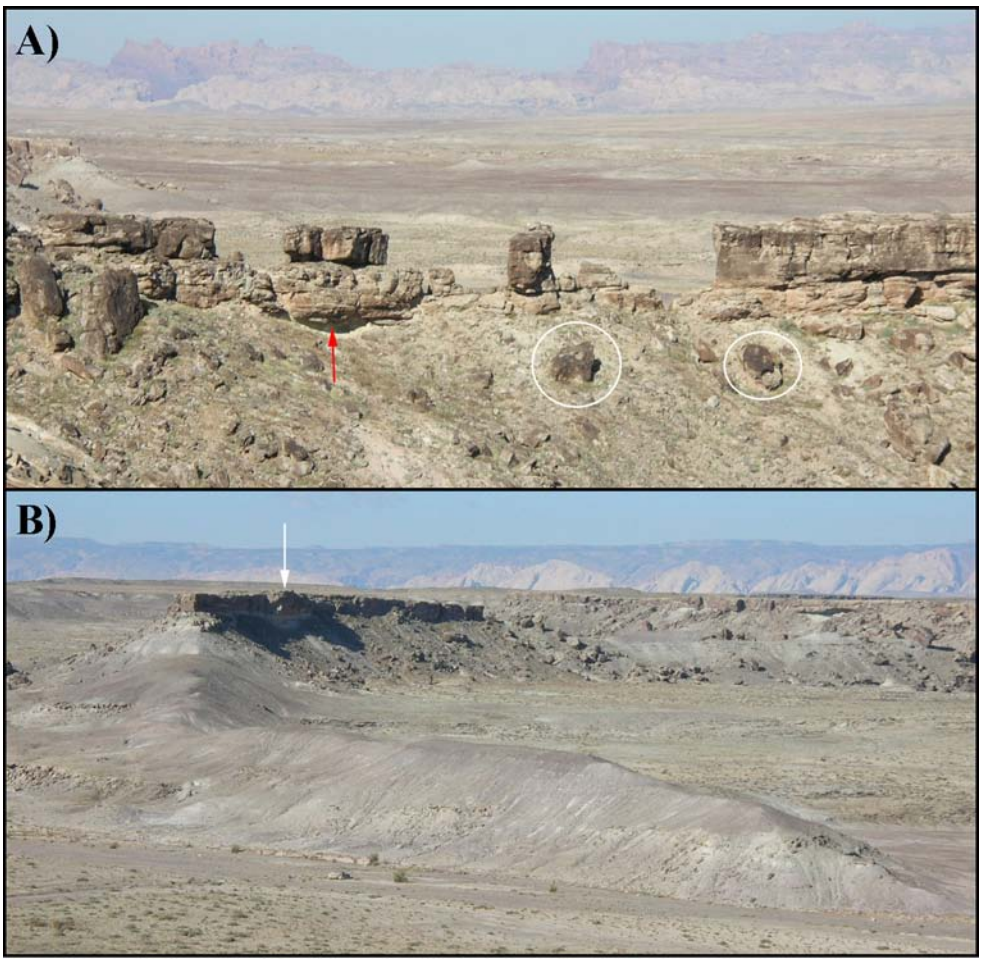

Supplemental Figure 12. A) Examples of degradation along sections of inverted paleochannels in the Ruby Ranch Member of the Cedar Mountain Formation. Erosion exploits the joints and faults in the paleochannels, producing blocks of cemented channel sediments. Blocks that have been transported downslope by mass wasting are marked by white circles. Differential erosion is also evident, with the underlying mudstone preferentially removed from beneath the more resistant paleochannels caprock; this undermining produces alcoves (red arrow). B) Cemented fluvial sediments form a capstone (white arrow). Where the capstone has been removed, the underlying mudstone still marks the original flow path (in this case curing around to the lower right in the image).

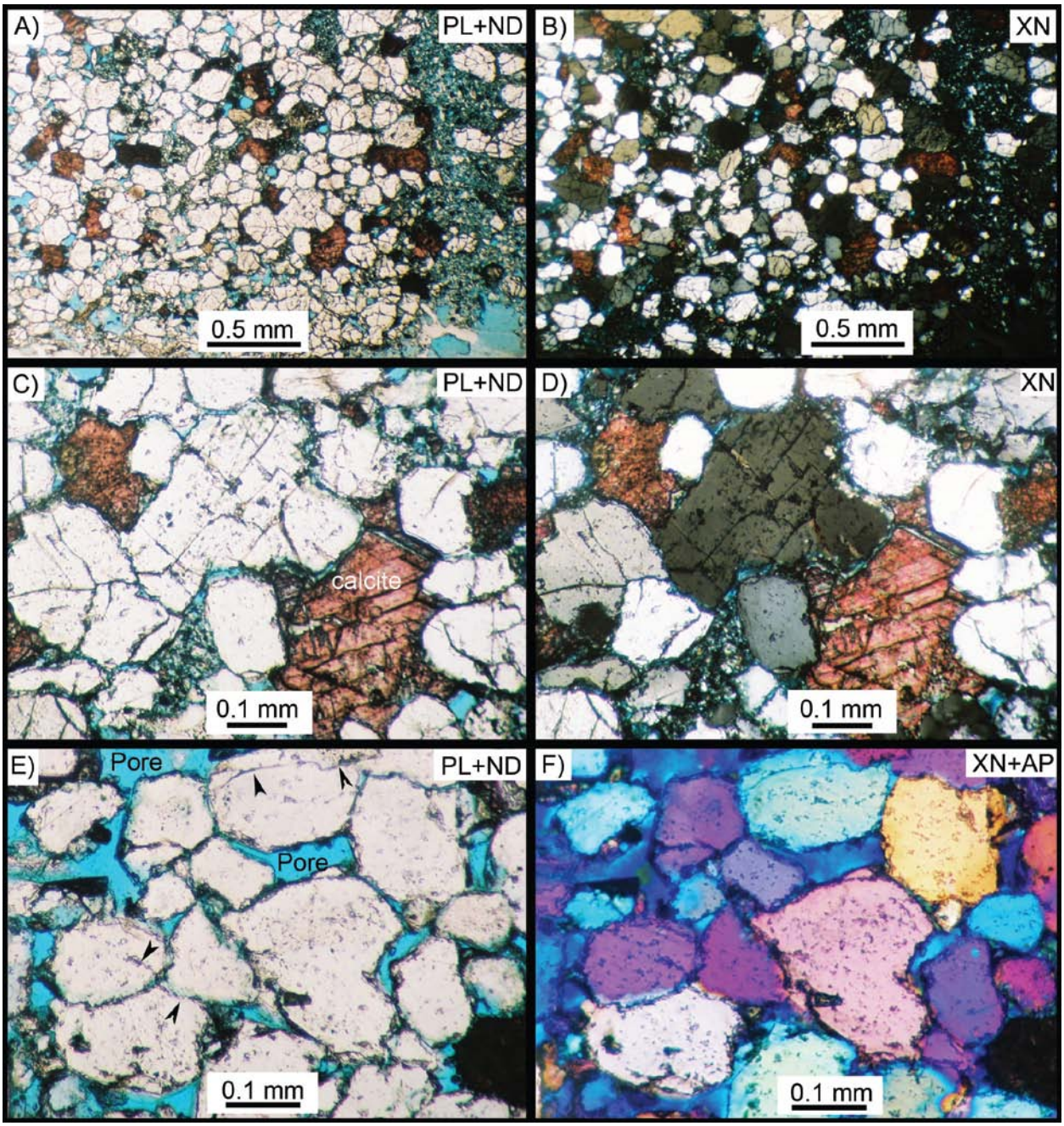

Supplemental Figure 13. Photomicrographs from samples of cemented channel materials in the Salt Wash Member of the Morrison Formation (stop 7; Figure 12). A) Quartz sandstone with silica overgrowth cements and minor calcite (red due to Alizarin Red-S stain) cement in plain light with neutral density filter. 50X. B) Same view as in previous figure with XN. 50X C) Sparry calcite (red) and silica cement around detrital quartz grains. 160X. D) Same view as in previous figure. 160X. E) Close-up view of dust lines (arrows) separating grains from silica cement. 200X. F) Same view as in previous figure. Optical continuity between grain and cement is evident under XN. 200X.

Supplemental Figure 14. View of the contact between cemented fluvial deposits and underlying red floodplain materials within the Salt Wash Member of the Morrison Formation. The capstone margin is near vertical and cut by fractures. Approximate outcrop thickness is 2.5 m. Photo by R. Williams.